

Multiple-Target Detection in Cell-Free Massive MIMO-Assisted ISAC

Mohamed Elfiatoure, Mohammadali Mohammadi, *Senior Member, IEEE*,
Hien Quoc Ngo, *Senior Member, IEEE*, and Michail Matthaiou, *Fellow, IEEE*

Abstract—We propose a distributed implementation for integrated sensing and communication (ISAC) backed by a massive multiple input multiple output (CF-mMIMO) architecture without cells. Distributed multi-antenna access points (APs) simultaneously serve communication users (UEs) and emit probing signals towards multiple specified zones for sensing. The APs can switch between communication and sensing modes, and adjust their transmit power based on the network settings and sensing and communication operations' requirements. By considering local partial zero-forcing and maximum-ratio-transmit precoding at the APs for communication and sensing, respectively, we first derive closed-form expressions for the spectral efficiency (SE) of the UEs and the mainlobe-to-average-sidelobe ratio (MASR) of the sensing zones. Then, a joint operation mode selection and power control design problem is formulated to maximize the SE fairness among the UEs, while ensuring specific levels of MASR for sensing zones. The complicated mixed-integer problem is relaxed and solved via successive convex approximation approach. We further propose a low-complexity design, where AP mode selection is designed through a greedy algorithm and then power control is designed based on this chosen mode. Our findings reveal that the proposed scheme can consistently ensure a sensing success rate of 100% for different network setups with a satisfactory fairness among all UEs.

Index Terms—Cell-free massive multiple-input multiple-output (CF-mMIMO), integrated sensing and communication (ISAC), mainlobe-to-average sensing ratio (MASR), spectral efficiency (SE).

I. INTRODUCTION

The advent of integrated sensing and communication (ISAC) marks a significant leap forward for the sixth generation (6G) of wireless technology, introducing a pivotal shift in the use of limited spectral resources [2], [3]. This innovative approach aims at enhancing both the radar sensing capabilities and communication efficiency, by assigning frequencies traditionally dedicated to sensing for wireless communication purposes as well. Such dual functionality supports high data-rate applications, contributing to the efficient utilization of

This work is a contribution by Project REASON, a UK Government funded project under the Future Open Networks Research Challenge (FONRC) sponsored by the Department of Science Innovation and Technology (DSIT). It was also supported by the U.K. Engineering and Physical Sciences Research Council (EPSRC) (grant No. EP/X04047X/1). The work of H. Q. Ngo was supported by the U.K. Research and Innovation Future Leaders Fellowships under Grant MR/X010635/1, and a research grant from the Department for the Economy Northern Ireland under the US-Ireland R&D Partnership Programme. The work of M. Mohammadi and M. Matthaiou was supported by the European Research Council (ERC) under the European Union's Horizon 2020 research and innovation programme (grant agreement No. 101001331).

The authors are with the Centre for Wireless Innovation (CWI), Queen's University Belfast, BT3 9DT Belfast, U.K., email:{melfiatoure01, m.mohammadi, hien.ngo, m.matthaiou}@qub.ac.uk. Parts of this paper appeared at the 2023 IEEE GLOBECOM conference [1].

spectral resources. ISAC's innovative framework has catalyzed the development of two distinct system architectures: separated systems and co-located systems. A separated system, also referred to as coexistence communication and radar, relies on distinct devices to perform radar sensing and communication within the same frequency band, generating sensing and communication beams independently. This method has been thoroughly investigated in our previous studies [4], [5] among others. In contrast, co-located systems, or dual-functional radar-communication (DFRC), integrate these functionalities within a single device. This allows for the simultaneous detection of radar targets and communication with multiple users (UEs), facilitated by an ISAC base station (BS) that utilizes shared hardware components for concurrent beam generation [6]. Recognized for its efficiency and cost-effectiveness, the DFRC architecture is heralded as a significant breakthrough for the beyond 5G (B5G) era, poised to redefine the network performance and optimization [7]–[9].

Transitioning from separated to co-located systems reflects an intention to streamline operational efficiency and reduce the complexity inherent in managing the exchange of side-information between radar and communication technologies [8], [9]. This evolution is notably supported by the integration of massive multiple-input multiple-output (mMIMO) technology, which particularly within co-located architectures, can effectively minimize the inter-user interference across the same time-frequency resources. Leveraging the substantial spatial degrees of freedom and intrinsic sensing capabilities, the fusion of mMIMO technology with ISAC is poised to deliver high-quality wireless communication, while ensuring high-resolution and robust sensing. Such advancements are instrumental in accelerating the development of various emerging applications, including, but not limited to, autonomous driving in intelligent transportation systems and unmanned aerial vehicle networks in smart cities [10], [11].

Expanding on this groundwork, recent research endeavors, as highlighted in studies by [12] and [13], have delved into the intricacies of a dual-functional system that marries communication and radar functionalities within an mMIMO orthogonal frequency division multiplexing (OFDM) architecture. These studies comprehensively address both downlink and uplink scenarios, offering insightful analytical derivations of the achievable rate and detection efficiency under various conditions of channel side information (CSI), encompassing both perfect and imperfect scenarios. Moreover, the work in [14] sought to optimize this dual-functional system. The focus was on maximizing the sum-rate and energy efficiency,

while ensuring compliance with essential operational parameters, including a baseline target detection probability and the satisfaction of individual UE rate demands.

Another powerful network topology is cell-free mMIMO (CF-mMIMO), which offers great potential to significantly improve the network connectivity. Diverging from traditional cellular setups that centralize all antennas at the BS, CF-mMIMO distributes antennas via the use of multiple access points (APs). These APs are then coordinated by several central processing units (CPUs), paving the way for a more distributed and flexible network architecture [15]–[18]. A CF-mMIMO ISAC topology has several advantages over the single-cell ISAC, including larger monitoring areas, broader sensing coverage, and a wider range of sensing angles. Nevertheless, in such systems, proper resource allocation plays a key role to facilitate both communication and sensing functionalities.

A. Related Works

Some recent papers have focused on integrating ISAC capabilities within CF-mMIMO. These studies aim to harness the benefits of both ISAC and CF-mMIMO technologies to further enhance the network performance and service delivery, as evidenced by works such as those in [19]–[23].

Among these contributions, Zeng *et al.* [19] made notable advancements in power allocation techniques within CF-mMIMO ISAC systems, optimizing the balance between communication and sensing functionalities. Behdad *et al.* [20] further explored the operational dynamics of CF-mMIMO ISAC systems, demonstrating how transmitting APs not only provide service to UEs but also partake in sensing operations for target location identification. Their research introduced a power distribution strategy that enhances the sensing signal-to-noise ratio (SNR) while adhering to signal-to-interference-plus-noise ratio (SINR) constraints for UEs. Building on these themes, Demirhan *et al.* [21] tackled the challenges of beamforming design in CF-mMIMO ISAC systems. They proposed a joint beamforming approach designed to maximize the sensing SNR without compromising the communication SINR, highlighting the critical balance required for effective sensing and communication within these networks. Additionally, the papers by Mao *et al.* [22] and Da *et al.* [23] have been instrumental in advancing precoder design for CF-mMIMO ISAC systems. These works also delved into the assessment of privacy risks associated with the inference of target locations by internal adversaries, marking a significant exploration beyond the technical aspects to include security and privacy considerations within ISAC networks.

B. Contributions

Contrary to the above studies, which assume static AP operation modes, our research introduces an innovative approach to CF-mMIMO ISAC networks by adopting dynamic AP operation mode selection. This novel strategy aims to optimize the spectral efficiency (SE) fairness among the UEs, while also ensuring the system’s capability to detect multiple designated targets. By leveraging long-term CSI, the APs are categorized

into communication APs (C-APs) and sensing APs (S-APs) to simultaneously support both downlink communication and sensing tasks. Compared to our recent work [1], where a single sensing zone area was considered and maximum ratio transmission (MRT) was performed at all APs, we consider a multiple sensing zone scenario and apply local partial zero-forcing (PZF) and MRT precoding at the C-APs and S-APs, respectively. The principle behind the PZF design is that each AP only suppresses the inter-UE interference it causes to the strongest UEs, namely the UEs with the largest channel gain, while the inter-UE interference caused to the weakest UEs is tolerated [24]. The main contributions of our paper can be summarized as follows:

- We develop a framework for analyzing the performance of a CF-mMIMO ISAC system with multiple C-APs and S-APs employing PZF and MRT precodings, respectively, under channel estimation errors. By leveraging the use-and-then-forget strategy, we derive closed-form expressions for the downlink SE of the communication UEs and mainlobe-to-average sensing ratio (MASR) of the sensing zones. We further pursue an asymptotic SE analysis, which discloses that when the number of C-APs and S-APs, denoted by M_c and M_s respectively, are large, we can scale down the transmit powers at the C-APs and S-APs proportionally to $1/M_c^2$ and $1/M_s^2$, respectively.
- We formulate an interesting problem of joint AP operation mode selection and power control design, considering per-AP power constraints and a MASR constraint for target detection in a multi-target environment. A new algorithm is developed to solve the challenging formulated mixed-integer non-convex problem. In particular, we transform the formulated problem into a more tractable problem with continuous variables only. Then, we solve the problem using successive convex approximation (SCA) techniques.
- To achieve a performance-complexity tradeoff, we propose a greedy algorithm for AP operation mode selection. This algorithm iteratively selects the optimal mode for each AP by considering the constraints for sensing operation, while maximizing fairness among UEs. Then, we propose a power control design algorithm for fixed AP operation mode design.
- Our numerical results show that the proposed joint algorithm can provide noticeable fairness among the UEs, while ensuring successful sensing performance for all sensing zones. The greedy algorithm achieves an acceptable level of success in the sensing rate.

A comparison of our contributions against the state of the art in the space of CF-mMIMO ISAC is tabulated in Table I.

C. Paper Organization and Notation

The rest of this paper is organized as follows: In Section II, we describe the system model for the proposed CF-mMIMO ISAC system with the corresponding communication and sensing metrics. In Section III, we analyze the per-UE SE in the asymptotic regime. The proposed AP mode selection and power allocation schemes are discussed in Section IV. Finally,

TABLE I: Contrasting our contributions to the mMIMO ISAC literature

Contributions	This paper	[19]	[20]	[21]	[22]
CF-mMIMO	✓	✓	✓	✓	✓
Power allocation	✓	✓	✓	✓	
Beamforming design	✓	✓	✓	✓	
AP operation mode selection	✓				
Multiple targets	✓				✓
Asymptotic analysis	✓				

the numerical results and some discussions are provided in Section V, followed by the conclusion remarks in Section VI.

Notation: We use bold lower (capital) case letters to denote vectors (matrices). The superscripts $(\cdot)^H$ and $(\cdot)^T$ stand for the Hermitian and transpose operation, respectively; \mathbf{I}_N denotes the $N \times N$ identity matrix; $\text{tr}(\cdot)$ and $(\cdot)^{-1}$ denote the trace operator and matrix inverse, respectively. A circular symmetric complex Gaussian distribution having variance σ^2 is denoted by $\mathcal{CN}(0, \sigma^2)$. Finally, $\mathbb{E}\{\cdot\}$ denotes the statistical expectation.

II. SYSTEM MODEL

We consider a CF-mMIMO ISAC system operating under time division duplex (TDD), where M APs serve K downlink UEs, while concurrently emitting probing signals towards L specific sensing zones. Each UE is equipped with a single antenna, and each AP deploys an array of N antennas. All APs and UEs function in a half-duplex mode. For the ease of exposition, we introduce the sets $\mathcal{M} \triangleq \{1, \dots, M\}$, $\mathcal{L} \triangleq \{1, \dots, L\}$, and $\mathcal{K} \triangleq \{1, \dots, K\}$ to represent the indices of the APs, sensing areas, and UEs, respectively. As depicted in Fig. 1, downlink communication and target detection are conducted concomitantly over the same frequency band. To accommodate the varying network demands, a dynamic AP operation mode selection strategy is implemented, determining the allocation of APs for downlink information transmission or radar sensing. A subset of APs, designated as communication-APs, termed as C-APs, is responsible for delivering information to the UEs. In contrast, the rest, labeled as S-APs, are employed for target detection. This categorization enables a specialized functionality of each AP group, where the C-APs aim to optimize the communication quality, while the S-APs enhance the radar sensing accuracy.

A. Channel Model and Uplink Training

We assume a quasi-static channel model, with each channel coherence interval spanning a duration of τ symbols. The duration of the training is denoted as τ_t , while the duration of downlink information transfer and target detection is $(\tau - \tau_t)$.

For the sensing channel model, we assume there is a line-of-sight (LoS) path between the sensing area and each AP, which is a commonly adopted model in the literature [20], [21]. The LoS channel between AP m and sensing area l is given by

$$\bar{\mathbf{g}}_{ml} = \mathbf{a}_N(\phi_{t,ml}^a, \phi_{t,ml}^e), \quad \forall m \in \mathcal{M}, \quad (1)$$

where $\phi_{t,ml}^a$, $\phi_{t,ml}^e$ denote the azimuth and elevation angles of departure (AoD) from AP m towards the sensing area l . Moreover, the q -th entry of the array response vector

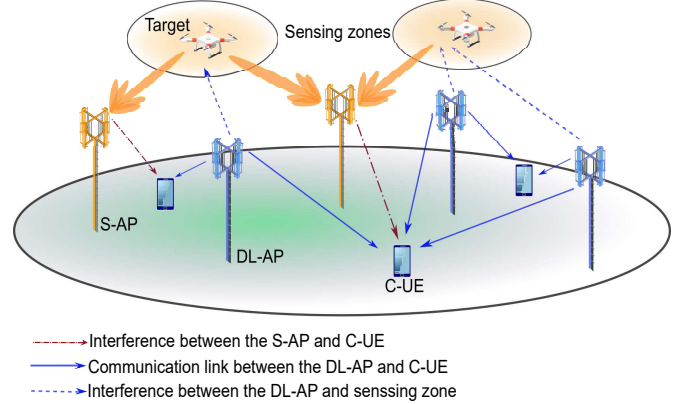


Fig. 1: Illustration of the CF-mMIMO ISAC system.

$\mathbf{a}_N(\phi_{t,ml}^a, \phi_{t,ml}^e) \in \mathbb{C}^{N \times 1}$, is given by

$$\begin{aligned} & [\mathbf{a}_N(\phi_{t,ml}^a, \phi_{t,ml}^e)]_q \\ &= \exp\left(j \frac{2\pi d}{\lambda} (q-1) \sin(\phi_{t,ml}^a) \cos(\phi_{t,ml}^e)\right), \end{aligned} \quad (2)$$

where d and λ denote the AP antenna spacing and carrier wavelength, respectively.

The channel vector between the m -th AP and k -th UE is modeled as $\mathbf{g}_{mk} = \sqrt{\beta_{mk}} \mathbf{h}_{mk}$, where β_{mk} is the large scale fading coefficient, while $\mathbf{h}_{mk} \in \mathbb{C}^{N \times 1}$ is the small-scale fading vector, whose elements are independent and identically distributed $\mathcal{CN}(0, 1)$ random variables (RVs).

An uplink training process is implemented to acquire the local CSI between each AP and all UEs. In each coherence block of length τ , all UEs are assumed to transmit their pairwise orthogonal pilot sequence of length τ_t to all APs, which requires $\tau_t \geq K$. At AP m , \mathbf{g}_{mk} is estimated by using the received pilot signals and applying the minimum mean-square error (MMSE) estimation technique. By following [17], the MMSE estimate $\hat{\mathbf{g}}_{mk}$ of \mathbf{g}_{mk} is obtained as $\hat{\mathbf{g}}_{mk} \sim \mathcal{CN}(\mathbf{0}, \gamma_{mk} \mathbf{I}_N)$, where

$$\gamma_{mk} = \frac{\tau_t \rho_t \beta_{mk}^2}{\tau_t \rho_t \beta_{mk} + 1}, \quad (3)$$

while ρ_t represents the normalized transmit power of each pilot symbol.

B. Probing and Data Signal Transmission

AP operation mode selection is performed by considering large-scale fading effects and relying on the statistical CSI. The binary variables used to indicate the operation mode for each AP m are defined as

$$a_m = \begin{cases} 1, & \text{if AP } m \text{ operates as C-AP} \\ 0, & \text{if AP } m \text{ operates as S-AP.} \end{cases} \quad (4)$$

The transmission phase comprises information transmission from the C-APs to UEs and probing signal transmission from the S-APs to the target. Let $\mathbf{x}_{c,m}$ and $\mathbf{x}_{r,m}$ denote the data and probing signals, respectively. The signal vector transmitted from AP m can be expressed as

$$\mathbf{x}_m = \sqrt{a_m} \mathbf{x}_{c,m} + \sqrt{(1-a_m)} \mathbf{x}_{r,m}. \quad (5)$$

The probing signal transmitted by the m -th S-AP, targeting specific sensing zones, can be expanded as

$$\mathbf{x}_{r,m} = \sum_{l \in \mathcal{L}} \sqrt{\rho \eta_{ml}^s} \mathbf{t}_{ml}^{\text{Sen}} x_{r,ml}, \quad (6)$$

where ρ denotes the maximum normalized downlink power; η_{ml}^s is the power control coefficient at S-AP m related to sensing zone l ; $\mathbf{t}_{ml}^{\text{Sen}} \in \mathbb{C}^{N \times 1}$ denotes the beamforming vector for sensing the l th sensing area, while $x_{r,ml}$, with $\mathbb{E}\{|x_{r,ml}|^2\} = 1$, is the radar sensing symbol from S-AP m for sensing the l th zone. This directional beamforming approach allows each S-AP to transmit a beam focused on a specific sector, facilitating spatially distributed sensing across the network. Therefore, to detect the presence of a target within its designated sector, each S-AP tailors its sensing beamforming vector to concentrate the radiated energy towards a specific direction. This is accomplished by configuring the beamforming vector to align with the azimuth and elevation angles that correspond to the sector of interest. Therefore, to detect the presence of a target in a certain location, we design the sensing beamforming vector at the m th S-AP as

$$\mathbf{t}_{ml}^{\text{Sen}} = \mathbf{a}_N(\phi_{t,ml}^a, \phi_{t,ml}^e). \quad (7)$$

This focused beamforming ensures that the radar echo from the target is sufficiently strong for reliable detection.

C. Downlink Communication and SE

In this section, we investigate the performance of partial zero forcing (PZF) precoding scheme. The conventional maximum ratio (MR) and ZF are special cases of PZF, and hence, their performances can be directly obtained from PZF.

PZF precoding emerges as an innovative method with the potential to combine the benefits of both ZF and MR approaches. The cornerstone of PZF lies in its ability to suppress interference caused to the strongest UEs, i.e., UEs with the highest channel gain, while tolerating the interference caused to the weakest UEs. In more detail, for any given AP (denoted as AP m), the set of active UEs is conceptually divided into two distinct subsets: (i) strong UEs, and (ii) weak UEs. The sets of indices for strong and weak UEs are represented as $\mathcal{S}_m \subset \{1, \dots, K\}$, and $\mathcal{W}_m \subset \{1, \dots, K\}$ respectively. It should be noted that $\mathcal{S}_m \cap \mathcal{W}_m = \emptyset$ and $|\mathcal{S}_m| + |\mathcal{W}_m| = K$. The grouping strategy can be determined using various criteria. For example, it may be based on the mean-square of the channel gain: a UE k is allocated to \mathcal{S}_m if β_{mk} exceeds a predetermined threshold, otherwise, k is placed in \mathcal{W}_m . PZF operates locally in the following manner: AP m transmits to all the UEs $k \in \mathcal{S}_m$ using ZF, and to all the UEs $k \in \mathcal{W}_m$ using MR.

The UE grouping can be based on different criteria. Inspired by [24], [25], the UE grouping strategy in PZF relies on the

following rule

$$\sum_{k=1}^{|\mathcal{S}_m|} \frac{\bar{\beta}_{mk}}{\sum_{t=1}^K \beta_{mt}} \geq \varrho\%, \quad (8)$$

where AP m constructs its set \mathcal{S}_m by selecting the UEs that contribute to, at least, $\varrho\%$ of the overall channel gain. Note that in (8), $\{\bar{\beta}_{m1}, \dots, \bar{\beta}_{mK}\}$ indicates the set of the large-scale fading coefficients sorted in descending order.

Therefore, transmit signal from AP m can be expressed as

$$\mathbf{x}_{c,m} = \left(\sum_{k \in \mathcal{S}_m} \sqrt{\rho \eta_{mk}^c} \mathbf{t}_{mk}^{\text{ZF-Com}} + \sum_{k \in \mathcal{W}_m} \sqrt{\rho \eta_{mk}^c} \mathbf{t}_{mk}^{\text{MR-Com}} \right) x_{c,k}, \quad (9)$$

where η_{mk}^c denotes the power control coefficient between C-AP m and UE k , $k \in \mathcal{K}$; $x_{c,k}$ is the communication symbol satisfying $\mathbb{E}\{|x_{c,k}|^2\} = 1$; $\mathbf{t}_{mk}^{\text{ZF-Com}}$ and $\mathbf{t}_{mk}^{\text{MR-Com}}$ represent the ZF and MR precoding vectors, respectively, given by

$$\mathbf{t}_{mk}^{\text{ZF-Com}} = \gamma_{mk} \hat{\mathbf{G}}_{\mathcal{S}_m} \left(\hat{\mathbf{G}}_{\mathcal{S}_m}^H \hat{\mathbf{G}}_{\mathcal{S}_m} \right)^{-1} \mathbf{e}_k \quad (10)$$

$$\mathbf{t}_{mk}^{\text{MR-Com}} = \hat{\mathbf{g}}_{mk}^*, \quad (11)$$

where \mathbf{e}_k is the k th column of $\mathbf{I}_{|\mathcal{S}_m|}$ and $\hat{\mathbf{G}}_{\mathcal{S}_m} = [\hat{\mathbf{g}}_{mk}^T : k \in \mathcal{S}_m]$. Therefore, for any pair of UEs k and k' belonging to the \mathcal{S}_m , we have

$$\hat{\mathbf{g}}_{mk'}^T \mathbf{t}_{mk}^{\text{ZF-Com}} = \begin{cases} \gamma_{mk} & \text{if } k = k', \\ 0 & \text{otherwise.} \end{cases} \quad (12)$$

The power control coefficients at AP m are chosen to satisfy the power constraint at each S-AP and C-AP, respectively, i.e.,

$$a_m \mathbb{E}\{\|\mathbf{x}_{c,m}\|^2\} + (1-a_m) \mathbb{E}\{\|\mathbf{x}_{r,m}\|^2\} \leq \rho. \quad (13)$$

For the sake of notation simplicity, we introduce \mathcal{Z}_k and \mathcal{M}_k as the set of indices of APs that transmit to UE k using $\mathbf{t}_{mk}^{\text{ZF-Com}}$ and $\mathbf{t}_{mk}^{\text{MR-Com}}$ respectively, given as

$$\mathcal{Z}_k \triangleq \{m : k \in \mathcal{S}_m, m = 1, \dots, M\}, \quad (14a)$$

$$\mathcal{M}_k \triangleq \{m : k \in \mathcal{W}_m, m = 1, \dots, M\}, \quad (14b)$$

with $\mathcal{Z}_k \cap \mathcal{M}_k = \emptyset$ and $\mathcal{Z}_k \cup \mathcal{M}_k = \mathcal{M}$. The PZF precoding approach provides a sophisticated balance between ZF and MR, catering to interference suppression for the strongest UEs and signal strength maximization for the weakest ones.

The received signal at the k -th UE can be represented as

$$\begin{aligned} y_k = & \left(\sum_{m \in \mathcal{Z}_k} \sqrt{a_m \rho \eta_{mk}^c} \mathbf{g}_{mk}^T \mathbf{t}_{mk}^{\text{ZF-Com}} \right. \\ & + \sum_{m \in \mathcal{M}_k} \sqrt{a_m \rho \eta_{mk}^c} \mathbf{g}_{mk}^T \mathbf{t}_{mk}^{\text{MR-Com}} \left. \right) x_{c,k} \\ & + \sum_{k' \in \mathcal{K} \setminus k} \left(\sum_{m \in \mathcal{Z}_k} \sqrt{a_m \rho \eta_{mk'}^c} \mathbf{g}_{mk'}^T \mathbf{t}_{mk'}^{\text{ZF-Com}} \right. \\ & + \sum_{m \in \mathcal{M}_k} \sqrt{a_m \rho \eta_{mk'}^c} \mathbf{g}_{mk'}^T \mathbf{t}_{mk'}^{\text{MR-Com}} \left. \right) x_{c,k'} \\ & + \sum_{m \in \mathcal{M}} \sum_{l \in \mathcal{L}} \sqrt{(1-a_m) \rho \eta_{ml}^s} \mathbf{g}_{mk}^T \mathbf{t}_{ml}^{\text{Sen}} x_{r,ml} + n_k, \end{aligned} \quad (15)$$

where the second term is the inter-user interference, the third term represents the interference from S-APs, and $n_k \sim \mathcal{CN}(0, 1)$ denotes the additive white Gaussian noise at the UE k . In order to apply the use-then-forget technique to derive the downlink SE at UE k , we rewrite (15) as

$$\begin{aligned} y_k = & \text{DS}_k x_{c,k} + \text{BU}_k x_{c,k} \\ & + \sum_{k' \in \mathcal{K} \setminus k} \text{IUI}_{kk'} x_{c,k'} + \text{IR}_k + n_k, \end{aligned} \quad (16)$$

where

$$\text{DS}_k \triangleq \mathbb{E} \left\{ \sum_{m \in \mathcal{Z}_k} \sqrt{a_m \rho \eta_{mk}^c} \mathbf{g}_{mk}^T \mathbf{t}_{mk}^{\text{ZF-Com}} + \sum_{m \in \mathcal{M}_k} \sqrt{a_m \rho \eta_{mk}^c} \mathbf{g}_{mk}^T \mathbf{t}_{mk}^{\text{MR-Com}} \right\} \quad (17a)$$

$$\text{BU}_k \triangleq \left(\sum_{m \in \mathcal{Z}_k} \sqrt{a_m \rho \eta_{mk}^c} \mathbf{g}_{mk}^T \mathbf{t}_{mk'}^{\text{ZF-Com}} + \sum_{m \in \mathcal{M}_k} \sqrt{a_m \rho \eta_{mk'}^c} \mathbf{g}_{mk'}^T \mathbf{t}_{mk'}^{\text{MR-Com}} \right) - \text{DS}_k, \quad (17b)$$

$$\text{IUI}_{kk'} \triangleq \sum_{m \in \mathcal{Z}_k} \sqrt{a_m \rho \eta_{mk'}^c} \mathbf{g}_{mk'}^T \mathbf{t}_{mk'}^{\text{ZF-Com}} + \sum_{m \in \mathcal{M}_k} \sqrt{a_m \rho \eta_{mk'}^c} \mathbf{g}_{mk'}^T \mathbf{t}_{mk'}^{\text{MR-Com}}, \quad (17c)$$

$$\text{IR}_k \triangleq \sum_{m \in \mathcal{M}} \sum_{l \in \mathcal{L}} \sqrt{(1 - a_m) \rho \eta_{ml}^s} \mathbf{g}_{mk}^T \mathbf{t}_{ml}^{\text{Sen}} x_{r,ml}, \quad (17d)$$

represent the strength of the desired signal (DS_k), the beam-forming gain uncertainty (BU_k), the interference caused by the k' -th UE ($\text{IUI}_{kk'}$) and the interference caused by S-APs (IR_k), respectively. By invoking (16), an achievable downlink SE at the k -th UE can be expressed as

$$\text{SE}_k = \left(1 - \frac{\tau_t}{\tau}\right) \log_2 (1 + \text{SINR}_k), \quad (18)$$

where $\text{SINR}_k =$

$$\frac{|\text{DS}_k|^2}{\mathbb{E}\{|\text{BU}_k|^2\} + \sum_{k' \in \mathcal{K} \setminus k} \mathbb{E}\{|\text{IUI}_{kk'}|^2\} + \mathbb{E}\{|\text{IR}_k|^2\} + 1}. \quad (19)$$

For the simplicity of notation, let us introduce a pair of binary variables to indicate the group assignment for each DL UE k and AP m in the PZF combining scheme as

$$\zeta_m^{\mathcal{Z}_k} = \begin{cases} 1 & \text{if } m \in \mathcal{Z}_k, \\ 0 & \text{otherwise.} \end{cases} \quad (20a)$$

$$\zeta_m^{\mathcal{M}_k} = \begin{cases} 1 & \text{if } m \in \mathcal{M}_k, \\ 0 & \text{otherwise.} \end{cases} \quad (20b)$$

Proposition 1. *The SE achieved by the PZF scheme is represented by (18), where SINR_k is given in (21) at the top of the next page.*

Proof: See Appendix B. \blacksquare

Remark 1. *Setting $\zeta_m^{\mathcal{M}_k} = 1$ and $\zeta_m^{\mathcal{Z}_k} = 0$, $\forall m \in \mathcal{M}$, results in the SINR given by (21) being reduced to that achieved by the MR precoding scheme. Similarly, if $\zeta_m^{\mathcal{M}_k} = 0$ and $\zeta_m^{\mathcal{Z}_k} = 1$, $\forall m \in \mathcal{M}$, the SINR in (21) reduces to that achieved by the ZF precoding scheme, provided that $N > K$.*

D. Sensing Operation and MASR

For a given angles $(\phi_{m \in \mathcal{M}}^a, \phi_{m \in \mathcal{M}}^e)$, the average spatial power pattern is

$$\begin{aligned} P_{\text{Com}}^{\text{ave}}(\phi_{m \in \mathcal{M}}^a, \phi_{m \in \mathcal{M}}^e) &= \mathbb{E} \left\{ \left| \sum_{m \in \mathcal{M}} \mathbf{a}_N^H(\phi_m^a, \phi_m^e) \mathbf{x}_m \right|^2 \right\} \\ &= \mathbb{E} \left\{ \underbrace{\left| \sum_{m \in \mathcal{M}} \sqrt{a_m} \mathbf{a}_N^H(\phi_m^a, \phi_m^e) \mathbf{x}_{c,m} \right|^2}_{\mathcal{T}_1} \right\} \\ &\quad + \mathbb{E} \left\{ \underbrace{\left| \sum_{m \in \mathcal{M}} \sqrt{(1 - a_m)} \mathbf{a}_N^H(\phi_m^a, \phi_m^e) \mathbf{x}_{r,m} \right|^2}_{\mathcal{T}_2} \right\}, \quad (22) \end{aligned}$$

where the expectation is taken over the transmitted signal \mathbf{x}_m and the small-scale fading.

Now, we proceed to derive \mathcal{T}_1 and \mathcal{T}_2 . By using (9), we can express \mathcal{T}_1 as

$$\begin{aligned} \mathcal{T}_1 &= \mathbb{E} \left\{ \left| \sum_{k \in \mathcal{K}} \left(\sum_{m \in \mathcal{Z}_k} \sqrt{a_m \rho \eta_{mk}^c} \mathbf{a}_N^H(\phi_m^a, \phi_m^e) \mathbf{t}_{mk}^{\text{ZF-Com}} + \sum_{m \in \mathcal{M}_k} \sqrt{a_m \rho \eta_{mk}^c} \mathbf{a}_N^H(\phi_m^a, \phi_m^e) \mathbf{t}_{mk}^{\text{MR-Com}} \right) \right|^2 \right\}, \\ &= \sum_{k \in \mathcal{K}} \left(\sum_{m \in \mathcal{Z}_k} a_m \rho \eta_{mk}^c \mathbb{E} \left\{ \left| \mathbf{a}_N^H(\phi_m^a, \phi_m^e) \mathbf{t}_{mk}^{\text{ZF-Com}} \right|^2 \right\} \right) \\ &\quad + \sum_{m \in \mathcal{M}_k} a_m \rho \eta_{mk}^c \mathbb{E} \left\{ \left| \mathbf{a}_N^H(\phi_m^a, \phi_m^e) \mathbf{t}_{mk}^{\text{MR-Com}} \right|^2 \right\}. \quad (23) \end{aligned}$$

By invoking Lemma 1 in Appendix A, we have

$$\begin{aligned} \mathcal{T}_1 &= \sum_{k \in \mathcal{K}} \left(\sum_{m \in \mathcal{Z}_k} a_m \rho \eta_{mk}^c \frac{\gamma_{mk}}{N - |\mathcal{S}_m|} \right. \\ &\quad \left. + \sum_{m \in \mathcal{M}_k} a_m \rho \eta_{mk}^c N \gamma_{mk} \right). \quad (24) \end{aligned}$$

Moreover, \mathcal{T}_2 can be obtained as

$$\mathcal{T}_2 = \rho \sum_{m \in \mathcal{M}} \sum_{l' \in \mathcal{L}} (1 - a_m) \eta_{ml'}^s \left| \mathbf{a}_N^H(\phi_m^a, \phi_m^e) \mathbf{t}_{ml'}^{\text{Sen}} \right|^2. \quad (25)$$

For the simplicity of notation, let us introduce a pair of binary variables to indicate the group assignment for each AP m and DL UE k , as

$$\delta_k^{\mathcal{S}_m} = \begin{cases} 1 & \text{if } k \in \mathcal{S}_m, \\ 0 & \text{otherwise.} \end{cases} \quad (26a)$$

$$\delta_k^{\mathcal{W}_m} = \begin{cases} 1 & \text{if } k \in \mathcal{W}_m, \\ 0 & \text{otherwise.} \end{cases} \quad (26b)$$

By invoking (22), the average spatial power pattern for sensing is given by

$$\begin{aligned} P_{\text{Com}}^{\text{ave}}(\phi_m^a, \phi_m^e) &= P_{\text{Com}}^{\text{ave}}(\phi_m^a, \phi_m^e) \\ &\quad + P_{\text{Sen}}^{\text{ave}}(\phi_m^a, \phi_m^e), \quad (27) \end{aligned}$$

where $P_{\text{Sen}}^{\text{ave}}(\phi_m^a, \phi_m^e) = \mathcal{T}_2$ represents power pattern related to L sensing zones, and $P_{\text{Com}}^{\text{ave}}(\phi_m^a, \phi_m^e) = \mathcal{T}_1$ represents the average sensing power distortion caused by simultaneous communication symbol transmissions in the network, given by

$$\begin{aligned} P_{\text{Com}}^{\text{ave}}(\phi_m^a, \phi_m^e) &= \rho \sum_{m \in \mathcal{M}} \sum_{k \in \mathcal{K}} a_m \eta_{mk}^c \gamma_{mk} \\ &\quad \times \left(\frac{\delta_k^{\mathcal{S}_m}}{N - |\mathcal{S}_m|} + N \delta_k^{\mathcal{W}_m} \right), \quad (28) \end{aligned}$$

which is independent of the angles.

Next, we consider the sensing performance associated with target l , i.e., at angle $(\phi_{t,ml}^a, \phi_{t,ml}^e)$ for all $m \in \mathcal{M}$. By using (25), $P_{\text{Sen}}^{\text{ave}}(\phi_{t,ml}^a, \phi_{t,ml}^e)$ can be expressed as

$$\begin{aligned} P_{\text{Sen}}^{\text{ave}}(\phi_{t,ml}^a, \phi_{t,ml}^e) &= \rho N^2 \sum_{m \in \mathcal{M}} (1 - a_m) \eta_{ml}^s \\ &\quad + \rho \sum_{m \in \mathcal{M}} \sum_{l' \in \mathcal{L} \setminus l} (1 - a_m) \eta_{ml'}^s \left| \mathbf{a}_N^H(\phi_{t,ml}^a, \phi_{t,ml}^e) \mathbf{t}_{ml'}^{\text{Sen}} \right|^2, \quad (29) \end{aligned}$$

where the first term denotes the desired power pattern for sensing at the angles related to target l and the second term is the average sensing power pattern distortion related to the other sensing zones.

It is desirable to have the average sensing power pattern distortion as well as $P_{\text{Com}}^{\text{ave}}(\phi_m^a, \phi_m^e)$, $\forall \phi_m^a$ and ϕ_m^e , as small as possible to confine the pattern distortion. Moreover, for

$$\text{SINR}_k(\mathbf{a}, \boldsymbol{\eta}^c, \boldsymbol{\eta}^s) = \frac{\rho \left(\sum_{m \in \mathcal{M}} \sqrt{a_m \eta_{mk}^c} \gamma_{mk} (\zeta_m^{\mathcal{Z}^k} + N \zeta_m^{\mathcal{M}^k}) \right)^2}{\rho \sum_{m \in \mathcal{M}} \sum_{k' \in \mathcal{K}} \left(a_m \eta_{mk'}^c \gamma_{mk'} \left(\zeta_m^{\mathcal{Z}^k} \frac{\beta_{mk} - \gamma_{mk}}{N - |\mathcal{S}_m|} + \zeta_m^{\mathcal{M}^k} N \beta_{mk} \right) \right) + \rho \sum_{m \in \mathcal{M}} \sum_{l \in \mathcal{L}} \eta_{ml}^s N (1 - a_m) \beta_{mk} + 1}, \quad (21)$$

illuminating a target angle $(\phi_{t,ml}^a, \phi_{t,ml}^e)$, it is desirable that the mainlobe level of desired term in $P_{\text{Sen}}^{\text{ave}}(\phi_{t,ml}^a, \phi_{t,ml}^e)$ is higher than the sum of sensing power pattern distortion and $P_{\text{Com}}^{\text{ave}}(\phi_m^a, \phi_m^e)$ by a certain minimum sensing level κ , $\forall \phi_m^a$ and ϕ_m^e , which is referred to as the MASR [26]. Accordingly, the MASR for the l th sensing zone is defined by (30) at the top of the next page. Note that, in general, in the MASR, we need to choose angles that maximize the average sensing power pattern distortion. However, this leads to an intractable MASR form. To alleviate such difficulty and make the MASR more amenable to further design, we choose $(\phi_{t,ml}^a, \phi_{t,ml}^e)$ for computing the sensing power pattern distortion in MASR. This is reasonable since we assume that we know the sensing zone l , and thus, we only need to search some directions around the angles of target l .

III. ASYMPTOTIC ANALYSIS

The system comprises a total of M APs. The APs are divided into two categories: M_c APs designated for communication activities and M_s APs dedicated to sensing tasks, ensuring the total AP count remains as $M = M_c + M_s$. With the application of MR precoding across all communication APs, we can pursue a detailed assessment of MR precoding's impact on the effectiveness of CF-mMIMO ISAC systems. In addition, we assume that equal power control is applied at the C-APs and S-APs, where

$$\eta_{mk}^c = \frac{1}{N \sum_{k' \in \mathcal{K}} \gamma_{mk'}}, \quad \forall k, \quad (31a)$$

$$\eta_{ml}^s = \frac{1}{NL}. \quad (31b)$$

We analyze the performance of two case studies: *i)* M is large and N is fixed, and; *ii)* N is large and M is fixed.

A. Case I ($M_s, M_c \rightarrow \infty$ and N is fixed)

In this section, we explore a scenario where both the numbers of APs designated for M_s and M_c approach infinity. Importantly, during this expansion, we maintain a constant ratio between M_c and M_s , symbolized as $c = \frac{M_c}{M_s}$. This examination sheds light on the system's asymptotic performance characteristics, when both the sensing and communication resources are scaled infinitely but proportionally. A critical aspect of this scenario involves the transmit power scaling of each AP. As M_c becomes very large, the transmit power per AP is adjusted according to $\rho = \frac{E}{M_c^2}$, where E is fixed. By applying (31) into (15), we have

$$\begin{aligned} y_k &= \sum_{m \in \mathcal{M}} \sqrt{\frac{a_m E}{N \sum_{k \in \mathcal{K}} \gamma_{mk}}} \frac{1}{M_c} \mathbf{g}_{mk}^T \mathbf{t}_{mk}^{\text{MR-Com}} x_{c,k} \\ &+ \sum_{k' \in \mathcal{K} \setminus k} \sum_{m \in \mathcal{M}} \sqrt{\frac{a_m E}{N \sum_{k \in \mathcal{K}} \gamma_{mk}}} \frac{1}{M_c} \mathbf{g}_{mk'}^T \mathbf{t}_{mk'}^{\text{MR-Com}} x_{c,k'} \\ &+ \sum_{m \in \mathcal{M}} \sum_{l \in \mathcal{L}} \sqrt{\frac{(1-a_m) E}{NL}} \frac{1}{c M_s} \mathbf{g}_{mk}^T \mathbf{t}_{ml}^{\text{Sen}} x_r + n_k. \end{aligned} \quad (32)$$

Then, by applying Tchebyshev's theorem we have¹

$$\begin{aligned} &\sum_{m \in \mathcal{M}} \sqrt{\frac{a_m E}{N \sum_{k \in \mathcal{K}} \gamma_{mk}}} \frac{1}{M_c} \mathbf{g}_{mk}^T \mathbf{t}_{mk}^{\text{MR-Com}} \\ &- \sum_{m \in \mathcal{M}} \sqrt{\frac{a_m N E}{\sum_{k \in \mathcal{K}} \gamma_{mk}}} \frac{\gamma_{mk}}{M_c} \xrightarrow{P} 0. \end{aligned} \quad (33)$$

Now, we turn our attention on the interference terms. For inter-user interference, by noting that the zero-mean channel vector \mathbf{g}_{mk} is independent of $\mathbf{t}_{mk'}^{\text{MR-Com}}$ for $k' \neq k$, we have

$$\sum_{m \in \mathcal{M}} \sqrt{\frac{a_m E}{N \sum_{k \in \mathcal{K}} \gamma_{mk}}} \frac{1}{M_c} \mathbf{g}_{mk}^T \mathbf{t}_{mk'}^{\text{MR-Com}} \xrightarrow{P} 0. \quad (34)$$

Moreover, for the deterministic $\mathbf{t}_{ml}^{\text{Sen}}$, we have

$$\sum_{m \in \mathcal{M}} \sum_{l \in \mathcal{L}} \sqrt{\frac{(1-a_m) E}{NL}} \frac{1}{c M_s} \mathbf{g}_{mk}^T \mathbf{t}_{ml}^{\text{Sen}} \xrightarrow{P} 0. \quad (35)$$

Accordingly, by using (33), (34), and (35), we have

$$y_k - \left(\sum_{m \in \mathcal{M}} \sqrt{\frac{a_m N E}{\sum_{k \in \mathcal{K}} \gamma_{mk}}} \frac{\gamma_{mk}}{M_c} \right) x_{c,k} \xrightarrow{P} 0. \quad (36)$$

The result in (36) indicates that when both M_c and M_s approach infinity, the received signal contains the desired signal plus noise. This indicates that inter-user interference and interference caused by S-APs fade, enhancing the signal quality. Most importantly, as M grows large, while the ratio of M_c and M_s is kept fixed, the transmit power at each AP can be made inversely proportional to the square of the number of APs with no degradation in performance.

B. Case II ($N \rightarrow \infty$ and M_c and M_s are fixed)

We explore the scenario where N approaches infinity, while M_c and M_s remain constant. The scaling of the transmit power for each AP is adjusted according to $\rho = \frac{E}{N}$, where E remains a fixed value.

By implementing the power scaling rule $\rho = \frac{E}{N}$, considering (15) and substituting $\mathbf{g}_{mk} = (\hat{\mathbf{g}}_{mk} + \tilde{\mathbf{g}}_{mk})$, the desired received signal at the UE can be characterized, as follows

$$\begin{aligned} &\sum_{m \in \mathcal{M}} \sqrt{\frac{a_m E}{\sum_{k \in \mathcal{K}} \gamma_{mk}}} \frac{1}{N} (\hat{\mathbf{g}}_{mk} + \tilde{\mathbf{g}}_{mk})^T \hat{\mathbf{g}}_{mk}^* \\ &\xrightarrow{a.s.} \sum_{m \in \mathcal{M}} \sqrt{\frac{a_m E}{\sum_{k \in \mathcal{K}} \gamma_{mk}}} \gamma_{mk}, \end{aligned} \quad (37)$$

where we have used the results on very long random vectors [28].

For the interference terms, noticing that \mathbf{g}_{mk}^T and $\mathbf{t}_{mk'}^{\text{MR-Com}}$

¹Let X_1, \dots, X_n be independent RVs, such that $\mathbb{E}\{X_i\} = \bar{x}_i$ and $\text{Var} \leq c \leq \infty$. Then, Tchebyshev's theorem states $\frac{1}{n} \sum_{n'=1}^n X_{n'} - \frac{1}{n} \sum_{n'} \bar{x}_{n'} \xrightarrow{P} 0$ [27].

$$\text{MASR}_l(\mathbf{a}, \boldsymbol{\eta}^c, \boldsymbol{\eta}^s) = \frac{\sum_{m \in \mathcal{M}} (1 - a_m) N^2 \eta_{ml}^s}{\sum_{m \in \mathcal{M}} \sum_{k \in \mathcal{K}} a_m \eta_{mk}^c \gamma_{mk} \left(\frac{\delta_k^{S_m}}{N - |\mathcal{S}_m|} + N \delta_k^{\mathcal{W}_m} \right) + \sum_{m \in \mathcal{M}} \sum_{l' \in \mathcal{L} \setminus l} (1 - a_m) \eta_{ml'}^s \left| \mathbf{a}_N^H(\phi_{t,ml}^a, \phi_{t,ml}^e) \mathbf{t}_{ml'}^{\text{sen}} \right|^2}. \quad (30)$$

are independent zero-mean vectors, we have

$$\sum_{m \in \mathcal{M}} \sqrt{\frac{a_m E}{\sum_{k \in \mathcal{K}} \gamma_{mk}}} \frac{1}{N} \mathbf{g}_{mk}^T \mathbf{t}_{mk'}^{\text{MR-Com}} \xrightarrow{a.s.} 0 \quad (38a)$$

$$\sum_{m \in \mathcal{M}} \sum_{l \in \mathcal{L}} \sqrt{\frac{(1 - a_m) E}{L}} \frac{1}{N} \mathbf{g}_{mk}^T \mathbf{t}_{ml}^{\text{Sen}} \xrightarrow{a.s.} 0. \quad (38b)$$

Then, by using (37) and (38) we have

$$y_k - \sum_{m \in \mathcal{M}} \sqrt{\frac{a_m E}{\sum_{k \in \mathcal{K}} \gamma_{mk}}} \gamma_{mk} x_{c,k} - n_k \xrightarrow{a.s.} 0, \text{ as } N \rightarrow \infty, \quad (39)$$

where $\xrightarrow{a.s.}$ denotes almost sure convergence. Akin to colocated mMIMO systems, the huge power gain (i.e. $\rho = \frac{E}{N}$) can be achieved, and the channels between the UEs and APs tend toward orthogonality as $N \rightarrow \infty$, elucidating the profound impact of deploying an extensive number of antennas in the CF-mMIMO ISAC space. This tendency towards channel orthogonality inherently mitigates the interference and enhances the signal quality, thereby reinforcing the premise that increasing the antenna count per AP not only avails of the advantages seen in traditional mMIMO architectures, but also significantly boosts the overall system performance and SE within the CF-mMIMO ISAC paradigm.

IV. PROPOSED DESIGN PROBLEMS AND SOLUTION

In this extended section, we formulate and solve the problem of joint AP mode selection and power allocation to provide fairness across the UEs, subject to quality of service (QoS) requirements of the sensing zone. More specifically, we aim to optimize the AP operation mode selection vector (\mathbf{a}) and power control coefficients ($\boldsymbol{\eta}_{mk}^c, \boldsymbol{\eta}_{ml}^s$) to maximize the minimum per-UE SE subject to a prescribed MASR level for the target detection and transmit power constraints at the APs.

In order to further simplify the optimization problem, we propose a greedy-based algorithm for AP mode selection and power control design. More specifically, the joint optimization problem is decomposed into two sub-problems: 1) AP mode selection, which is performed via a greedy algorithm and 2) Power control design for fixed AP modes.

Note that AP m is required to meet the average normalized power constraint, i.e., $\mathbb{E} \{ \|\mathbf{x}_{c,m}\|^2 \} \leq \rho$. By invoking (13), and noticing that $\mathbb{E} \{ \|\mathbf{t}_{mk}^{\text{ZF-Com}}\|^2 \} = \frac{\gamma_{mk}}{N - |\mathcal{S}_m|}$, we have the following per-AP power constraint

$$\sum_{k \in \mathcal{S}_m} \eta_{mk}^c \frac{\gamma_{mk}}{N - |\mathcal{S}_m|} + \sum_{k \in \mathcal{W}_m} N \gamma_{mk} \eta_{mk}^c \leq a_m. \quad (40)$$

A. Joint AP Mode Selection and Power Allocation Design

In this subsection, we formulate and solve the problem of joint AP mode selection and power control design. Define $\mathbf{a} \triangleq \{a_1, \dots, a_M\}$, $\boldsymbol{\eta}^c \triangleq \{\eta_{m1}^c, \dots, \eta_{mK}^c\}$ and $\boldsymbol{\eta}^s \triangleq$

$\{\eta_{m1}^s, \dots, \eta_{mL}^s\}$ for all $m \in \mathcal{M}$. The optimization problem is then formulated as

$$(\mathbf{P1}): \max_{\mathbf{a}, \boldsymbol{\eta}^c, \boldsymbol{\eta}^s} \min_{k \in \mathcal{K}} \text{SINR}_k(\mathbf{a}, \boldsymbol{\eta}^c, \boldsymbol{\eta}^s) \quad (41a)$$

$$\text{s.t. } \text{MASR}_l(\mathbf{a}, \boldsymbol{\eta}^c, \boldsymbol{\eta}^s) \geq \kappa, \forall l \in \mathcal{L}, \quad (41b)$$

$$\sum_{k \in \mathcal{S}_m} \eta_{mk}^c \frac{\gamma_{mk}}{N - |\mathcal{S}_m|} + \sum_{k \in \mathcal{W}_m} N \gamma_{mk} \eta_{mk}^c \leq a_m, \forall m \in \mathcal{M}, \quad (41c)$$

$$\sum_{l \in \mathcal{L}} \eta_{ml}^s \leq \frac{(1 - a_m)}{N}, \forall m \in \mathcal{M}, \quad (41d)$$

$$a_m \in \{0, 1\}, \quad (41e)$$

where the first constraint (41b) is to explicitly control the level of the MASR for all sensing zones, while the second and third constraint control the transmit power at the C-APs and S-APs, respectively.

Before proceeding, we introduce an auxiliary variable $t = \min_{k \in \mathcal{K}} \text{SINR}_k(\mathbf{a}, \boldsymbol{\eta}^c, \boldsymbol{\eta}^s)$. We further relax the binary constraint (41e). Since at the optimal point $a_m \in \{0, 1\}$, we replace a_m with a_m^2 in the second and third constraint to accelerate the convergence speed of the optimization problem. Accordingly, the optimization problem (41) is reformulated as follows:

$$(\mathbf{P2}): \max_{\mathbf{a}, \boldsymbol{\eta}^c, \boldsymbol{\eta}^s, t} t - \lambda \sum_{m \in \mathcal{M}} a_m - a_m^{(n)} \left(2a_m - a_m^{(n)} \right) \quad (42a)$$

$$\text{s.t. } \text{SINR}_k(\mathbf{a}, \boldsymbol{\eta}^c, \boldsymbol{\eta}^s) \geq t, \forall k \in \mathcal{K} \quad (42b)$$

$$\text{MASR}_l(\mathbf{a}, \boldsymbol{\eta}^c, \boldsymbol{\eta}^s) \geq \kappa, \forall l \in \mathcal{L}, \quad (42c)$$

$$\sum_{k \in \mathcal{S}_m} \eta_{mk}^c \frac{\gamma_{mk}}{N - |\mathcal{S}_m|} + \sum_{k \in \mathcal{W}_m} N \gamma_{mk} \eta_{mk}^c \leq a_m^{(n)} \left(2a_m - a_m^{(n)} \right), \forall m \in \mathcal{M}, \quad (42d)$$

$$\sum_{l \in \mathcal{L}} \eta_{ml}^s \leq \frac{(1 - a_m^2)}{N}, \forall m \in \mathcal{M}, \quad (42e)$$

$$0 \leq a_m \leq 1, \forall m \in \mathcal{M}. \quad (42f)$$

The non-convex nature of constraints (42b) and (42c) make the resulting problem non-convex. To address the non-convexity, we employ the method of SCA. To deal with the non-convexity of (42b), we first define

$$\varrho_{mk} \triangleq \zeta_m^{\mathcal{Z}_k} \frac{(\beta_{mk} - \gamma_{mk})}{N - |\mathcal{S}_m|} + \zeta_m^{\mathcal{M}_k} N \beta_{mk}, \quad (43a)$$

$$f_{mk} \triangleq \zeta_m^{\mathcal{Z}_k} + N \zeta_m^{\mathcal{M}_k}. \quad (43b)$$

Now, constraint (42b) can be expressed as

$$\frac{\left(\sum_{m \in \mathcal{M}} \sqrt{a_m \rho \eta_{mk}^c} \gamma_{mk} f_{mk} \right)^2}{\sum_{m \in \mathcal{M}} a_m \left(\sum_{k' \in \mathcal{K}} \eta_{mk'}^c \gamma_{mk'} \varrho_{mk} - \sum_{l \in \mathcal{L}} \eta_{ml}^s N \beta_{mk} \right)} \geq t$$

$$+ \rho \sum_{m \in \mathcal{M}} \sum_{l \in \mathcal{L}} \eta_{ml}^s N \beta_{mk} + 1. \quad (44)$$

For ease of description, let us denote

$$\mu_{mk} \triangleq \sum_{k' \in \mathcal{K}} \eta_{mk'}^c \gamma_{mk'} \varrho_{mk} - \sum_{l \in \mathcal{L}} \eta_{ml}^s N \beta_{mk}. \quad (45)$$

To this end, (44) is equivalent to

$$\begin{aligned} & \frac{\left(2 \sum_{m \in \mathcal{M}} \sqrt{a_m \eta_{mk}^c} \gamma_{mk} f_{mk}\right)^2}{t} + \sum_{m \in \mathcal{M}} (a_m - \mu_{mk})^2 \\ & \geq \sum_{m \in \mathcal{M}} (a_m + \mu_{mk})^2 + 4 \sum_{m \in \mathcal{M}} \sum_{l \in \mathcal{L}} \eta_{ml}^s N \beta_{mk} + 4/\rho. \end{aligned} \quad (46)$$

It is clear that we need to find a concave lower bound of the left-hand side of the above inequality. To this end, we note that the function x^2/y is convex for $y > 0$, and thus, the following inequality holds

$$\frac{x^2}{y} \geq \frac{x_0}{y_0} \left(2x - \frac{x_0}{y_0} y\right), \quad (47)$$

which is obtained by linearizing x^2/y around x_0 and y_0 . Let us now define

$$q_k^{(n)} \triangleq \frac{2 \sum_{m \in \mathcal{M}} \sqrt{a_m^{(n)} (\eta_{mk}^c)^{(n)} \gamma_{mk} f_{mk}}}{t^{(n)}}. \quad (48)$$

From the inequality (47), we can recast (46) as

$$\begin{aligned} & q_k^{(n)} \left(4 \sum_{m \in \mathcal{M}} \sqrt{a_m \eta_{mk}^c} \gamma_{mk} f_{mk} - q_k^{(n)} t\right) \\ & + \sum_{m \in \mathcal{M}} (a_m^{(n)} - \mu_{mk}^{(n)}) \left(2(a_m - \mu_{mk}) - (a_m^{(n)} - \mu_{mk}^{(n)})\right) \\ & \geq \sum_{m \in \mathcal{M}} (a_m + \mu_{mk})^2 \\ & \quad + 4 \sum_{m \in \mathcal{M}} \sum_{l \in \mathcal{L}} \eta_{ml}^s N \beta_{mk} + 4/\rho, \end{aligned} \quad (49)$$

where we have used the following inequality

$$x^2 \geq x_0(2x - x_0), \quad (50)$$

and replaced x and x_0 by $a_m - \mu_{mk}$ and $a_m^{(n)} - \mu_{mk}^{(n)}$, respectively.

Now, we focus on (42c), which can be expressed as

$$\begin{aligned} & \sum_{m \in \mathcal{M}} (1 - a_m) N^2 \eta_{ml}^s \\ & \geq \kappa \sum_{m \in \mathcal{M}} \sum_{l' \in \mathcal{L} \setminus l} (1 - a_m) \eta_{ml'}^s \left| \mathbf{a}_N^H(\phi_{t,ml}^a, \phi_{t,ml}^e) \mathbf{t}_{ml'}^{\text{sen}} \right|^2 \\ & + \kappa \sum_{m \in \mathcal{M}} \sum_{k \in \mathcal{K}} a_m \eta_{mk}^c \gamma_{mk} \theta_{mk}, \end{aligned} \quad (51)$$

where $\theta_{mk} \triangleq \frac{\delta_k^{S_m}}{N - |S_m|} + N \delta_k^{\mathcal{W}_m}$. Now, we can recast (51) as

$$\begin{aligned} & \sum_{m \in \mathcal{M}} N^2 \eta_{ml}^s \geq \\ & \sum_{m \in \mathcal{M}} a_m \left(N^2 \eta_{ml}^s + \kappa \sum_{k \in \mathcal{K}} \eta_{mk}^c \gamma_{mk} \theta_{mk} \right. \\ & \left. - \kappa \sum_{l' \in \mathcal{L} \setminus l} \eta_{ml'}^s \left| \mathbf{a}_N^H(\phi_{t,ml}^a, \phi_{t,ml}^e) \mathbf{t}_{ml'}^{\text{sen}} \right|^2 \right) \\ & + \kappa \sum_{m \in \mathcal{M}} \sum_{l' \in \mathcal{L} \setminus l} \eta_{ml'}^s \left| \mathbf{a}_N^H(\phi_{t,ml}^a, \phi_{t,ml}^e) \mathbf{t}_{ml'}^{\text{sen}} \right|^2. \end{aligned} \quad (52)$$

For ease of description let us denote

$$\begin{aligned} \nu_{ml} & \triangleq \left(N^2 \eta_{ml}^s + \kappa \sum_{k \in \mathcal{K}} \eta_{mk}^c \gamma_{mk} \theta_{mk} \right. \\ & \left. - \kappa \sum_{l' \in \mathcal{L} \setminus l} \eta_{ml'}^s \left| \mathbf{a}_N^H(\phi_{t,ml}^a, \phi_{t,ml}^e) \mathbf{t}_{ml'}^{\text{sen}} \right|^2 \right). \end{aligned} \quad (53)$$

Accordingly, (52) can be written as

$$\begin{aligned} & 4 \sum_{m \in \mathcal{M}} N^2 \eta_{ml}^s + \sum_{m \in \mathcal{M}} (a_m - \nu_{ml})^2 \geq \\ & \sum_{m \in \mathcal{M}} (a_m + \nu_{ml})^2 \\ & + 4\kappa \sum_{m \in \mathcal{M}} \sum_{l' \in \mathcal{L} \setminus l} \eta_{ml'}^s \left| \mathbf{a}_N^H(\phi_{t,ml}^a, \phi_{t,ml}^e) \mathbf{t}_{ml'}^{\text{sen}} \right|^2. \end{aligned} \quad (54)$$

Algorithm 1 Proposed algorithm for joint AP mode selection and power allocation design (JAP-PA)

- 1: **Initialize:** $n=0$, $\lambda > 1$, a random initial point $\tilde{\mathbf{x}}^{(0)} \in \hat{\mathcal{F}}$.
- 2: **repeat**
- 3: Update $n = n + 1$
- 4: Solve (56) to obtain its optimal solution $\tilde{\mathbf{x}}^*$
- 5: Update $\tilde{\mathbf{x}}^{(n)} = \tilde{\mathbf{x}}^*$
- 6: **until** convergence

To this end, by using (50), we obtain the concave lower bound of the left-hand side of the above inequality. Then, we get

$$\begin{aligned} & 4 \sum_{m \in \mathcal{M}} N^2 \eta_{ml}^s + \sum_{m \in \mathcal{M}} (a_m^{(n)} - \nu_{ml}^{(n)}) \\ & \times \left(2(a_m - \nu_{ml}) - (a_m^{(n)} - \nu_{ml}^{(n)}) \right) \geq \sum_{m \in \mathcal{M}} (a_m + \nu_{ml})^2 \\ & + 4\kappa \sum_{m \in \mathcal{M}} \sum_{l' \in \mathcal{L} \setminus l} \eta_{ml'}^s \left| \mathbf{a}_N^H(\phi_{t,ml}^a, \phi_{t,ml}^e) \mathbf{t}_{ml'}^{\text{sen}} \right|^2. \end{aligned} \quad (55)$$

Now, the convex optimization problem is given as (56), at the top of the next page. Problem **(P3)** is a convex optimization problem and can be efficiently solved using CVX [29]. In **Algorithm 1**, we outline main steps to solve problem **(P3)**, where $\tilde{\mathbf{x}} \triangleq \{\mathbf{a}, \boldsymbol{\eta}^c, \boldsymbol{\eta}^s\}$ and $\hat{\mathcal{F}} \triangleq \{(56b), (56c), (56d), (56e), (56f)\}$ is a convex feasible set. Starting from a random point $\tilde{\mathbf{x}} \in \hat{\mathcal{F}}$, we solve (56) to obtain its optimal solution $\tilde{\mathbf{x}}^*$, and use $\tilde{\mathbf{x}}^*$ as an initial point in the next iteration. The proof of this convergence property uses similar steps as the proof of [30, Proposition 2], and hence, is omitted herein due to lack of space.

Complexity of Algorithm 1: **Algorithm 1** requires solving a series of convex problems (56). For ease of presentation, if we let $K = L$, problem (56) can be transformed to an equivalent problem that involves $A_v \triangleq (M + 2MK + 1)$ real-valued scalar variables, $A_l \triangleq 3M$ linear constraints, $A_q \triangleq 2K$ quadratic constraints. Therefore, the algorithm for solving problem (56) requires a complexity of $\mathcal{O}(\sqrt{A_l + A_q}(A_v + A_l + A_q)A_v^2)$ in each iteration [31], [32]. In Section V, we will show that this algorithm converges to the optimal solution after a few iterations.

B. Greedy AP Mode Selection and Optimized Power Allocation

In this subsection, to reduce the complexity of the joint optimization problem, while maintaining an acceptable system performance, we propose a greedy algorithm to determine the operation modes of the APs. Then, given the operation modes of the APs, we jointly optimize the power control coefficients for the C-APs and S-APs.

1) *Greedy AP Mode Selection:* Let \mathcal{A}_{Sen} and \mathcal{A}_{Com} denote the sets containing the indices of APs operating as radar, i.e., APs with $a_m = 0$, and of APs operating in communication mode, i.e., APs with $a_m = 1$, respectively. In addition, $\text{MASR}_l(\mathcal{A}_{\text{Sen}}, \mathcal{A}_{\text{Com}})$ and $\text{SINR}_k(\mathcal{A}_{\text{Sen}}, \mathcal{A}_{\text{Com}})$ underline the dependence of the sensing MASR (of the l -th zone) and received SINR (of the k -th UE) on the different choices of AP mode selection. Our greedy algorithm of AP mode selection is shown in **Algorithm 2**. To guarantee the sensing MASR requirement, all APs are initially assigned for sensing operation, i.e., $\mathcal{A}_{\text{Sen}} = \mathcal{M}$ and $\mathcal{A}_{\text{Com}} = \emptyset$. Then, in each

$$\text{(P3): } \max_{\mathbf{a}, \boldsymbol{\eta}^c, \boldsymbol{\eta}^s, t} t - \lambda \sum_{m \in \mathcal{M}} a_m - a_m^{(n)} (2a_m - a_m^{(n)}) \quad (56a)$$

$$\begin{aligned} \text{s.t. } & q_k^{(n)} \left(4 \sum_{m \in \mathcal{M}} \sqrt{a_m \eta_{mk}^c} \gamma_{mk} f_{mk} - q_k^{(n)} t \right) + \sum_{m \in \mathcal{M}} (a_m^{(n)} - \mu_{mk}^{(n)}) \left(2(a_m - \mu_{mk}) - (a_m^{(n)} - \mu_{mk}^{(n)}) \right) \\ & \geq \sum_{m \in \mathcal{M}} (a_m + \mu_{mk})^2 + 4 \sum_{m \in \mathcal{M}} \sum_{l \in \mathcal{L}} \eta_{ml}^s N \beta_{mk} + 4/\rho, \end{aligned} \quad (56b)$$

$$\begin{aligned} & 4 \sum_{m \in \mathcal{M}} N^2 \eta_{ml}^s + \sum_{m \in \mathcal{M}} (a_m^{(n)} - \nu_{ml}^{(n)}) \left(2(a_m - \nu_{ml}) - (a_m^{(n)} - \nu_{ml}^{(n)}) \right) \\ & \geq \sum_{m \in \mathcal{M}} (a_m + \nu_{ml})^2 + 4\kappa \sum_{m \in \mathcal{M}} \sum_{l' \in \mathcal{L} \setminus l} \eta_{ml'}^s \left| \mathbf{a}_N^H (\phi_{t,ml}^a, \phi_{t,ml}^e) \mathbf{t}_{ml'}^{\text{sen}} \right|^2, \end{aligned} \quad (56c)$$

$$\sum_{k \in \mathcal{S}_m} \eta_{mk}^c \frac{\gamma_{mk}}{N - |\mathcal{S}_m|} + \sum_{k \in \mathcal{W}_m} N \gamma_{mk} \eta_{mk}^c \leq a_m^{(n)} (2a_m - a_m^{(n)}), \forall m \in \mathcal{M}, \quad (56d)$$

$$\sum_{l \in \mathcal{L}} \eta_{ml}^s \leq \frac{(1 - a_m^2)}{N}, \forall m \in \mathcal{M}, \quad (56e)$$

$$0 \leq a_m \leq 1. \quad (56f)$$

iteration, one AP switches into communication operation mode for maximizing the minimum SE (or equivalently SINR), while the minimum MARSs, required for target sensing, in all sensing zones are guaranteed. This process continues until there is no more improvement in the minimum SINR across all UEs.

2) *Power Allocation*: For a given operation mode selection vector (\mathbf{a}) , we optimize the power control coefficients $(\boldsymbol{\eta}_{mk}^c, \boldsymbol{\eta}_{ml}^s)$ to achieve maximum fairness among the EUs. Therefore, the optimization problem (41) is reduced to

$$\text{(P4): } \max_{\boldsymbol{\eta}^c, \boldsymbol{\eta}^s} t \quad (57a)$$

$$\text{s.t. } \text{SINR}_k(\boldsymbol{\eta}^c, \boldsymbol{\eta}^s) \geq t, \quad (57b)$$

$$\text{MASR}_l(\boldsymbol{\eta}^c, \boldsymbol{\eta}^s) \geq \kappa, \forall l \in \mathcal{L}, \quad (57c)$$

$$\begin{aligned} & \sum_{k \in \mathcal{S}_m} \eta_{mk}^c \frac{\gamma_{mk}}{N - |\mathcal{S}_m|} \\ & + \sum_{k \in \mathcal{W}_m} N \gamma_{mk} \eta_{mk}^c \leq a_m, \forall m \in \mathcal{M}, \end{aligned} \quad (57d)$$

$$\sum_{l \in \mathcal{L}} \eta_{ml}^s \leq \frac{(1 - a_m)}{N}, \forall m \in \mathcal{M}. \quad (57e)$$

We note that constraints (57b) and (57c) are non-convex. To deal with this non-convexity, we first introduce the auxiliary variables $\xi_{mk}^2 = \eta_{mk}^c$, which yields the optimization problem (58), at the middle of the next page.

At the next step, we replace the convex function in the numerator of (58b) with its concave lower bound, which results in the following constraint

$$\frac{z_k^{(n)} \left(2 \sum_{m \in \mathcal{M}} \sqrt{a_m} \xi_{mk} \gamma_{mk} f_{mk} - z_k^{(n)} \right)}{\Delta(\boldsymbol{\xi}, \boldsymbol{\eta}^s)} \geq t, \quad (59)$$

where $\Delta(\boldsymbol{\xi}, \boldsymbol{\eta}^s) \triangleq \rho \sum_{m \in \mathcal{M}} a_m \varrho_{mk} \sum_{k' \in \mathcal{K}} \xi_{mk'}^2 \gamma_{mk'} + \rho \sum_{m \in \mathcal{M}} N(1 - a_m) \beta_{mk} \sum_{l \in \mathcal{L}} \eta_{ml}^s + 1$ and $z_k^{(n)} \triangleq \sum_{m \in \mathcal{M}} \sqrt{a_m} \xi_{mk}^{(n)} \gamma_{mk} f_{mk}$. Therefore, the power control design problem for fixed AP mode operation is given by

$$\text{(P6): } \max_{\boldsymbol{\xi}, \boldsymbol{\eta}^s, t} t \quad (60a)$$

$$\text{s.t. } (59), (58c) - (58e), \quad (60b)$$

The optimization problem in (60) is again convex, which we can solve directly using the bisection technique and solving linear feasibility problems, as shown in **Algorithm 3**.

Algorithm 2 Greedy AP Mode Selection

- 1: **Initialize**: Set $\mathcal{A}_{\text{Com}} = \emptyset$ and $\mathcal{A}_{\text{Sen}} = \mathcal{M}$. Set iteration index $i = 0$.
 - 2: Calculate $\Pi^*[i] = \min_{k \in \mathcal{K}} \text{SE}_k(\mathcal{A}_{\text{Sen}}, \mathcal{A}_{\text{Com}})$
 - 3: **repeat**
 - 4: **for all** $m \in \mathcal{A}_{\text{Sen}}$ **do**
 - 5: Set $\mathcal{A}_s = \mathcal{A}_{\text{Sen}} \setminus m$.
 - 6: **if** $\text{MASR}_l(\mathcal{A}_s, \mathcal{A}_{\text{Com}} \cup m) \geq \kappa, \forall l \in \mathcal{L}$ **then**
 - 7: Calculate $\Pi_m = \min_{k \in \mathcal{K}} \text{SINR}_k(\mathcal{A}_s, \mathcal{A}_{\text{Com}} \cup m)$
 - 8: **else**
 - 9: Set $\Pi_m = 0$
 - 10: **end if**
 - 11: **end for**
 - 12: Set $\Pi^*[i+1] = \max_{m \in \mathcal{A}_{\text{Com}}} \Pi_m$
 - 13: $e = |\Pi^*[i+1] - \Pi^*[i]|$
 - 14: **if** $e \geq e_{\min}$ **then**
 - 15: Update $\mathcal{A}_{\text{Com}} = \{\mathcal{A}_{\text{Com}} \cup m^*\}$ and $\mathcal{A}_{\text{Sen}} = \mathcal{A}_{\text{Sen}} \setminus m^*$
 - 16: **end if**
 - 17: Set $i = i + 1$
 - 18: **until** $e < e_{\min}$
 - 19: **return** \mathcal{A}_{Sen} and \mathcal{A}_{Com} , i.e., the indices of APs operating in radar mode and communication mode, respectively.
-

Algorithm 3 Bisection algorithm for solving (60)

- (1) *Initialization*: Choose the initial values of t_{\max} and t_{\min} , where t_{\max} and t_{\min} define a range of objective function values. Set tolerance $\epsilon > 0$.
 - (2) Set $t := \frac{t_{\max} + t_{\min}}{2}$ and solve the convex feasibility problem (60).
 - (3) If the problem in Step 2 is feasible, set $t_{\min} := t$; else set $t_{\max} := t$.
 - (5) Stop if $t_{\max} - t_{\min} < \epsilon$. Otherwise, go to Step 2.
-

Remark 2. It is important to note that, for a given network realization, it is likely that the greedy and/or random AP selection schemes cannot guarantee the sensing requirement in the network design. Hence, we introduce a new metric known as the **success sensing rate**, defined as the ratio of the number of network realizations with successful sensing for all sensing zones to the total number of channel realizations. For

$$\text{(P5): } \max_{\xi, \eta^s, t} t \quad (58a)$$

$$\text{s.t. } \frac{\left(\sum_{m \in \mathcal{M}} \sqrt{\rho a_m} \xi_{mk} \gamma_{mk} f_{mk} \right)^2}{\rho \sum_{m \in \mathcal{M}} a_m Q_{mk} \sum_{k' \in \mathcal{K}} \xi_{mk'}^2 \gamma_{mk'} + \rho \sum_{m \in \mathcal{M}} N(1-a_m) \beta_{mk} \sum_{l \in \mathcal{L}} \eta_{ml}^s + 1} \geq t, \quad (58b)$$

$$\frac{\sum_{m \in \mathcal{M}} a_m \sum_{k \in \mathcal{K}} \xi_{mk}^2 \gamma_{mk} \theta_{mk} + \sum_{m \in \mathcal{M}} (1-a_m) \sum_{l \in \mathcal{L} \setminus l} \eta_{ml}^s \left| \mathbf{a}_N^H(\phi_{t,ml}^a, \phi_{t,ml}^e) \mathbf{t}_{ml}^{\text{sen}} \right|^2}{\sum_{m \in \mathcal{M}} (1-a_m) N^2 \eta_{ml}^s} \geq \kappa, \quad \forall l \in \mathcal{L}, \quad (58c)$$

$$\sum_{k \in \mathcal{K}} \xi_{mk}^2 \gamma_{mk} \theta_{mk} \leq a_m, \quad \forall m \in \mathcal{M}, \quad (58d)$$

$$\sum_{l \in \mathcal{L}} \eta_{ml}^s \leq \frac{(1-a_m)}{N}, \quad \forall m \in \mathcal{M}, \quad (58e)$$

a fair comparison, in each channel realization, if the MASR requirements are not met or the optimization problem of a scheme is infeasible, we set the SE of that scheme to zero.

V. NUMERICAL EXAMPLES

In this section, we verify the correctness of our analytical results and the performance of the proposed algorithms.

A. Large-scale Fading Model and System Parameters

We assume that the M APs and K UEs are uniformly distributed in a square of 0.5×0.5 km², whose edges are wrapped around to avoid the boundary effects. The large-scale fading coefficients β_{mk} are modeled as [33]

$$\beta_{mk} [\text{dB}] = -30.5 - 36.7 \log_{10} \left(\frac{d_{mk}}{1 \text{ m}} \right) + F_{mk}, \quad (61)$$

where d_{mk} is the distance between UE k and AP m (computed as the minimum over different wrap-around cases) and $F_{mk} \sim \mathcal{CN}(0, 4^2)$ is the shadow fading. The shadowing terms from an AP to different UEs are correlated, as

$$\mathbb{E}\{F_{mk} F_{jk'}\} \triangleq \begin{cases} 4^{2-\delta_{kk'}/9 \text{ m}}, & \text{if } j = m, \\ 0, & \text{otherwise,} \end{cases} \quad (62)$$

where $\delta_{kk'}$ is the physical distance between UEs k and k' .

The values of the network parameters are $\tau = 200$, and $\tau_t = K + L$. We further set the bandwidth $B = 50$ MHz and noise figure $F = 9$ dB. Thus, the noise power $\sigma_n^2 = k_B T_0 B F$, where $k_B = 1.381 \times 10^{-23}$ Joules/^oK is the Boltzmann constant, while $T_0 = 290$ °K is the noise temperature. Let $\tilde{\rho} = 1$ W, and $\tilde{\rho}_t = 0.25$ W be the maximum transmit power of the APs and uplink training pilot sequences, respectively. The normalized maximum transmit powers ρ and ρ_t are calculated by dividing these powers by the noise power.

To evaluate the performance of proposed AP mode selection schemes, we consider random AP selection with optimized power allocation (**RAP-OPA**). In the numerical results, **JAP-OPA** denotes our proposed design in Algorithm 1, i.e., joint AP mode selection and power allocation design. Moreover, greedy AP selection and optimized power allocation design is indicated by **GAP-OPA**.

B. Results and Discussions

The empirical cumulative distributed functions (CDFs) of the per-UE SE for all scenarios with $\kappa = 8$ dB, $MN = 480$, $K = 4$ and $L = 2$ are plotted in Fig. 2. The bar chart

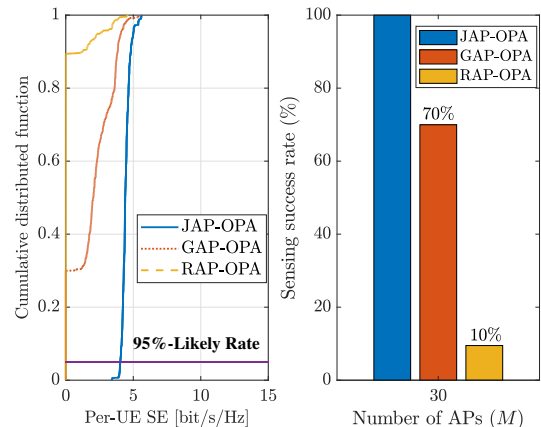


Fig. 2: CDF of the per-UE SE and sensing success rate ($\kappa = 8$ dB, $M = 30$, $N = 16$, $K = 4$, and $L = 2$).

corresponds to the sensing success rate of different schemes. It can be observed that while **JAP-OPA** guarantees the sensing requirement for all network realizations, **RAP-OPA** fails to meet this requirement, with a success rate of 10%. In other words, the power allocation problem becomes infeasible in 90% of cases. On the other hand, **GAP-OPA** yields comparable results, achieving a success rate of approximately 70%, which confirms the effectiveness of the proposed greedy algorithm. For the infeasible cases, according to our discussion in Remark 2, we set the SE of the UEs to zero. By comparing the CDFs of the per-UE SE across all schemes, we observe that **JAP-OPA** provides a satisfactory fairness among the UEs. Moreover, the SE achieved by **JAP-OPA** is much higher than that of the **GAP-OPA** and **RAP-OPA**.

Figure 3 shows the worst SE (minimum SE) across the UEs for given realizations of the large-scale fading coefficients and for two different number of sensing zones: $L = 3$ (dashed lines) and $L = 2$ (solid lines). The proposed **JAP-OPA** scheme significantly improves the worst SE over the benchmarks and provides 100% sensing success rate for both scenarios. Moreover, we observe that joint optimization can guarantee nearly the same minimum SE per UE across all different channel realizations, while random and greedy AP selection provides varying levels of per-UE SE. For example, when $L = 2$, in 60% of channel realizations, the minimum SE obtained via **GAP-OPA** is less than 3 bit/s/Hz, while **JAP-OPA** consistently provides a minimum SE greater than 4 bit/s/Hz. Moreover, by increasing the number of sensing zones

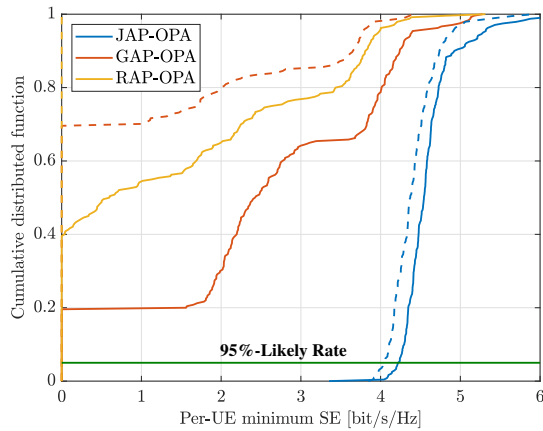


Fig. 3: CDF of the per-UE minimum SE for different schemes and for different number of sensing zones. The dashed lines depict results for $L = 3$ while the solid lines show results for $L = 2$ ($\kappa = 6$ dB, $M = 30$, $N = 16$, $K = 4$).

from 2 to 3, the sensing performance of both the **GAP-OPA** and **RAP-OPA** severely degraded, resulting in success rates of 27% and 1% for **GAP-OPA** and **RAP-OPA**, respectively. These findings confirm the importance of joint AP mode selection and power allocation for both communication and sensing operations.

Figure 4 shows the average of the minimum SE per-UE with a fixed number of antenna units in the network versus the number of APs. By increasing the number of APs, the proposed **JAP-OPA** outperforms all other schemes, while **RAP-OPA** yields the worst performance in terms of SE. Moreover, the sensing success rate of **GAP-OPA** and **RAP-OPA** decreases as the number of APs increases. It is most likely for **RAP-OPA** to fail when $M > 30$. This behavior is due to the fact that the MASR heavily depends on N , (it is proportional to N^2 according to (30)). Therefore, the MASR decreases significantly as M increases, and both **RAP-OPA** and **GAP-OPA** schemes cannot guarantee to meet the sensing requirement under this condition. Conversely, the proposed **JAP-OPA** scheme ensures successful sensing for all network realizations, while delivering much higher per-UE minimum SE compared to the **RAP-OPA** and **GAP-OPA** schemes. Interestingly, the SE performance of the the proposed **JAP-OPA** scheme is improved by increasing the number of APs. These results reveal the importance of joint AP mode selection and power control design in dense CF-mMIMO networks.

Figure 5 illustrates the average of the minimum SE per-UE versus κ , along with the sensing success rate of different schemes as a function of κ . As the sensing requirements increase, the sensing success rate of the **RAP-OPA** and **GAP-OPA** schemes decreases, particularly when $\kappa > 8$ dB. Additionally, the minimum SE per-UE sharply decreases for these two schemes. However, the proposed **JAP-OPA** scheme continues to meet the MASR requirements and delivers high values for the minimum per-UE . Figure 5 illustrates the average of the minimum SE per-UE versus κ , along with the sensing success rate of different schemes as a function of κ . As the sensing requirements increase, the sensing success rate of the **RAP-OPA** and **GAP-OPA** schemes decreases,

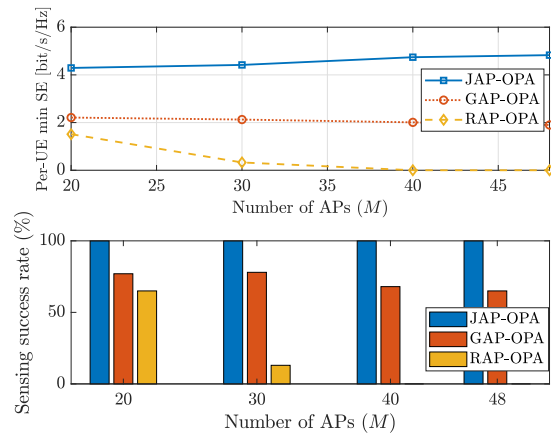


Fig. 4: Average of the per-UE minimum SE and sensing success rate versus the number of APs ($\kappa = 8$ dB, $MN = 480$, $K = 4$, and $L = 2$).

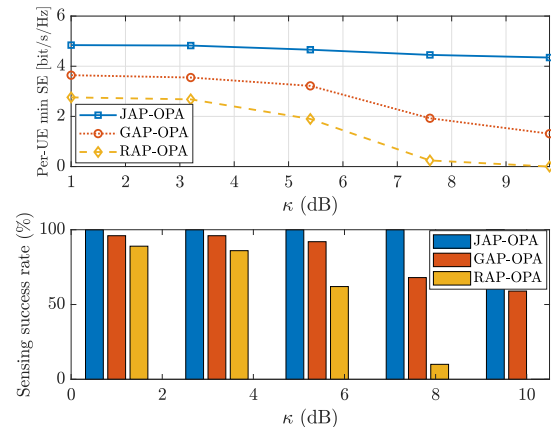


Fig. 5: Average of the per-UE minimum SE and sensing success rate versus κ ($MN = 480$, $M = 30$, $K = 4$, and $L = 2$).

particularly when $\kappa > 8$ dB. Additionally, the minimum SE per-UE sharply decreases for these two schemes. However, the proposed **JAP-OPA** continues to meet the MASR requirements and delivers high values for the minimum per-UE SE.

In Fig. 6, we compare the convergence rate of **Algorithm 1** for different number of APs in the network. To solve (56), we use the convex conic solver MOSEK and set $\lambda = 10$. We can see that with a small number of iterations (less than 60 iterations), **Algorithm 1** returns the optimized solution. The transient behavior stems from the penalty term $\lambda \sum_{m \in \mathcal{M}} a_m - a_m^{(n)} (2a_m - a_m^{(n)})$ in the optimization problem. Furthermore, it is worth mentioning that the resulting values of the parameters a_m converge to 1 and 0 with high accuracy.

VI. CONCLUSION

In this paper, we proposed a distributed ISAC implementation underpinned by a CF-mMIMO architecture. We analyzed both the exact and asymptotic SE performance of the downlink communication system and provided exact results for the MASR metric of the sensing zones. The operation mode of the distributed APs and their transmit power coefficients were jointly optimized to maximize fairness among communication

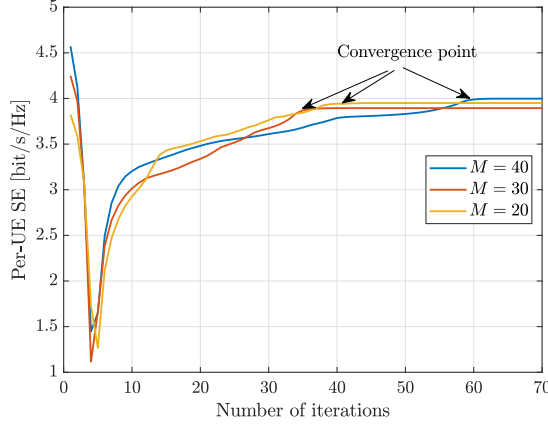


Fig. 6: Convergence behavior of **Algorithm 1** ($MN = 480$, $K = 4$, $L = 2$, $\lambda = 10$).

UEs, while ensuring a specific level of MASR for different sensing zones in the network. To reduce the computational complexity of the proposed optimal scheme, a low-complexity design was also developed, wherein the operation mode of the APs was determined through a greedy algorithm and then the transmit power of the APs was optimized via a bisection algorithm. The proposed AP mode selection and power control design has shown to provide significant performance over the benchmark systems with random/greedy AP mode selection for both communication and sensing operations.

APPENDIX A USEFUL LEMMA

Lemma 1. For the ZF beamforming vector $\mathbf{t}_{mk}^{\text{ZF-Com}}$, defined in (10), we have

$$\mathbb{E}\left\{\mathbf{t}_{mk}^{\text{ZF-Com}}(\mathbf{t}_{mk}^{\text{ZF-Com}})^H\right\} = \frac{\gamma_{mk}}{N(N-|\mathcal{S}_m|)}\mathbf{I}_N. \quad (63)$$

Proof: We first define $\mathbf{Q} \triangleq \hat{\mathbf{G}}_{\mathcal{S}_m}(\hat{\mathbf{G}}_{\mathcal{S}_m}^H \hat{\mathbf{G}}_{\mathcal{S}_m})^{-1}$ and $\mathbf{q}_k = \mathbf{Q}\mathbf{e}_k$, which is the k th column of $\mathbf{Q} \in \mathbb{C}^{N \times |\mathcal{S}_m|}$. Then, we have

$$\gamma_{mk}^2 \mathbb{E}\left\{\mathbf{q}_k \mathbf{q}_k^H\right\} = \frac{\gamma_{mk}^2}{|\mathcal{S}_m|} \sum_{k'=1}^{|\mathcal{S}_m|} \mathbb{E}\left\{\mathbf{q}_k \mathbf{q}_{k'}^H\right\}. \quad (64)$$

Accordingly, we have

$$\begin{aligned} \mathbb{E}\left\{\mathbf{t}_{mk}^{\text{ZF-Com}}(\mathbf{t}_{mk}^{\text{ZF-Com}})^H\right\} &= \frac{\gamma_{mk}^2}{|\mathcal{S}_m|} \mathbb{E}\left\{\mathbf{Q}\mathbf{Q}^H\right\} \\ &= \frac{\gamma_{mk}^2}{|\mathcal{S}_m|} \mathbb{E}\left\{\hat{\mathbf{G}}_{\mathcal{S}_m}(\hat{\mathbf{G}}_{\mathcal{S}_m}^H \hat{\mathbf{G}}_{\mathcal{S}_m})^{-1}(\hat{\mathbf{G}}_{\mathcal{S}_m}^H \hat{\mathbf{G}}_{\mathcal{S}_m})^{-1} \hat{\mathbf{G}}_{\mathcal{S}_m}^H\right\}. \end{aligned} \quad (65)$$

Let $\mathbf{B} = \mathbb{E}\left\{\hat{\mathbf{G}}_{\mathcal{S}_m}(\hat{\mathbf{G}}_{\mathcal{S}_m}^H \hat{\mathbf{G}}_{\mathcal{S}_m})^{-1}(\hat{\mathbf{G}}_{\mathcal{S}_m}^H \hat{\mathbf{G}}_{\mathcal{S}_m})^{-1} \hat{\mathbf{G}}_{\mathcal{S}_m}^H\right\}$. For any $N \times N$ unitary matrix Ω , we have

$$\Omega \mathbf{B} \Omega^H = \mathbb{E}\left\{\Omega \hat{\mathbf{G}}_{\mathcal{S}_m}(\hat{\mathbf{G}}_{\mathcal{S}_m}^H \hat{\mathbf{G}}_{\mathcal{S}_m})^{-1}(\hat{\mathbf{G}}_{\mathcal{S}_m}^H \hat{\mathbf{G}}_{\mathcal{S}_m})^{-1} \hat{\mathbf{G}}_{\mathcal{S}_m}^H \Omega^H\right\}. \quad (66)$$

Now, we define $\bar{\mathbf{G}}_{\mathcal{S}_m} = \Omega \hat{\mathbf{G}}_{\mathcal{S}_m}$. Thus, using (66), we have

$$\Omega \mathbf{B} \Omega^H = \mathbb{E}\left\{\bar{\mathbf{G}}_{\mathcal{S}_m}(\bar{\mathbf{G}}_{\mathcal{S}_m}^H \bar{\mathbf{G}}_{\mathcal{S}_m})^{-1}(\bar{\mathbf{G}}_{\mathcal{S}_m}^H \bar{\mathbf{G}}_{\mathcal{S}_m})^{-1} \bar{\mathbf{G}}_{\mathcal{S}_m}^H\right\}, \quad (67)$$

where we have used

$$\bar{\mathbf{G}}_{\mathcal{S}_m}^H \bar{\mathbf{G}}_{\mathcal{S}_m} = \hat{\mathbf{G}}_{\mathcal{S}_m}^H \Omega^H \Omega \hat{\mathbf{G}}_{\mathcal{S}_m} = \hat{\mathbf{G}}_{\mathcal{S}_m}^H \hat{\mathbf{G}}_{\mathcal{S}_m}. \quad (68)$$

Since $\bar{\mathbf{G}}_{\mathcal{S}_m} = \Omega \hat{\mathbf{G}}_{\mathcal{S}_m}$ is statistically identical to $\hat{\mathbf{G}}_{\mathcal{S}_m}$, we have $\Omega \mathbf{B} \Omega^H = \mathbf{B}$, for any unitary matrix Ω . By using an eigenvalue decomposition, \mathbf{B} can be expressed as

$\mathbf{B} = \mathbf{W}\mathbf{D}_\lambda\mathbf{W}^H$, where \mathbf{W} is a unitary matrix and \mathbf{D}_λ is a diagonal matrix. Then, $\Omega \mathbf{B} \Omega^H = \mathbf{B}$ is equivalent to

$$\Omega \mathbf{W} \mathbf{D}_\lambda \Omega^H \mathbf{W}^H = \mathbf{U} \mathbf{D}_\lambda \mathbf{U}^H = \mathbf{B}. \quad (69)$$

Since (69) is true for any unitary \mathbf{U} , \mathbf{B} must be a scaled identity matrix. This implies that $\mathbf{B} = c_1 \mathbf{I}_N$, where c_1 is a constant, given by

$$\begin{aligned} c_1 &= \frac{1}{N} \mathbb{E}\left\{\text{tr}\left(\hat{\mathbf{G}}_{\mathcal{S}_m}(\hat{\mathbf{G}}_{\mathcal{S}_m}^H \hat{\mathbf{G}}_{\mathcal{S}_m})^{-1}(\hat{\mathbf{G}}_{\mathcal{S}_m}^H \hat{\mathbf{G}}_{\mathcal{S}_m})^{-1} \hat{\mathbf{G}}_{\mathcal{S}_m}^H\right)\right\} \\ &= \frac{1}{N} \mathbb{E}\left\{\text{tr}\left(\hat{\mathbf{G}}_{\mathcal{S}_m}^H \hat{\mathbf{G}}_{\mathcal{S}_m}\right)^{-1}\right\} \\ &= \frac{|\mathcal{S}_m|}{N(N-|\mathcal{S}_m|)\gamma_{mk}}. \end{aligned} \quad (70)$$

APPENDIX B PROOF OF PROPOSITION 1

We first present the desired signal term as

$$\begin{aligned} \text{DS}_k &= \mathbb{E}\left\{\sum_{m \in \mathcal{Z}_k} \sqrt{a_m \rho \eta_{mk}^c} (\hat{\mathbf{g}}_{mk} + \tilde{\mathbf{g}}_{mk})^T \mathbf{t}_{mk}^{\text{ZF-Com}} \right. \\ &\quad \left. + \sum_{m \in \mathcal{M}_k} \sqrt{a_m \rho \eta_{mk}^c} (\hat{\mathbf{g}}_{mk} + \tilde{\mathbf{g}}_{mk})^T \mathbf{t}_{mk}^{\text{MR-Com}}\right\} \\ &= \sum_{m \in \mathcal{Z}_k} \sqrt{a_m \rho \eta_{mk}^c} \gamma_{mk} + N \sum_{m \in \mathcal{M}_k} \sqrt{a_m \rho \eta_{mk}^c} \gamma_{mk}, \end{aligned} \quad (71)$$

where we have used the fact that $\mathbf{t}_{mk}^{\text{ZF-Com}}$, $\mathbf{t}_{mk}^{\text{MR-Com}}$ and $\tilde{\mathbf{g}}_{mk}$ are zero mean and independent. In addition, the variance of the sum of independent RVs is equal to the sum of the variances. We can now proceed with the following derivation

$$\begin{aligned} \mathbb{E}\left\{|\text{BU}_k|^2\right\} &= \mathbb{E}\left\{\left|\sum_{m \in \mathcal{Z}_k} \sqrt{a_m \rho \eta_{mk}^c} \mathbf{g}_{mk}^T \mathbf{t}_{mk}^{\text{ZF-Com}} \right. \right. \\ &\quad \left. \left. + \sum_{m \in \mathcal{M}_k} \sqrt{a_m \rho \eta_{mk}^c} \mathbf{g}_{mk}^T \mathbf{t}_{mk}^{\text{MR-Com}}\right|^2\right\} - \text{DS}_k. \end{aligned} \quad (72)$$

We notice that

$$\begin{aligned} \vartheta &= \mathbb{E}\left\{\left|\sum_{m \in \mathcal{Z}_k} \sqrt{a_m \rho \eta_{mk}^c} \mathbf{g}_{mk}^T \mathbf{t}_{mk}^{\text{ZF-Com}} \right. \right. \\ &\quad \left. \left. + \sum_{m \in \mathcal{M}_k} \sqrt{a_m \rho \eta_{mk}^c} \mathbf{g}_{mk}^T \mathbf{t}_{mk}^{\text{MR-Com}}\right|^2\right\} \\ &= \vartheta_Z + \vartheta_M + 2\left(\sum_{m \in \mathcal{Z}_k} \sqrt{a_m \rho \eta_{mk}^c} \gamma_{mk}\right) \\ &\quad \times \left(N \sum_{m \in \mathcal{M}_k} \sqrt{a_m \rho \eta_{mk}^c} \gamma_{mk}\right), \end{aligned} \quad (73)$$

where

$$\begin{aligned} \vartheta_Z &= \mathbb{E}\left\{\left|\sum_{m \in \mathcal{Z}_k} \sqrt{a_m \rho \eta_{mk}^c} \mathbf{g}_{mk}^T \mathbf{t}_{mk}^{\text{ZF-Com}}\right|^2\right\} \\ \vartheta_M &= \mathbb{E}\left\{\left|\sum_{m \in \mathcal{M}_k} \sqrt{a_m \rho \eta_{mk}^c} \mathbf{g}_{mk}^T \mathbf{t}_{mk}^{\text{MR-Com}}\right|^2\right\}. \end{aligned} \quad (74)$$

We first focus on ϑ_Z , which can be obtained as

$$\begin{aligned} \vartheta_Z &= \mathbb{E}\left\{\left|\sum_{m \in \mathcal{Z}_k} \sqrt{a_m \rho \eta_{mk}^c} (\hat{\mathbf{g}}_{mk} + \tilde{\mathbf{g}}_{mk})^T \mathbf{t}_{mk}^{\text{ZF-Com}}\right|^2\right\} \\ &= \sum_{m \in \mathcal{Z}_k} a_m \rho \eta_{mk}^c \\ &\quad \times \mathbb{E}\left\{(\mathbf{t}_{mk}^{\text{ZF-Com}})^H \mathbb{E}\left\{\tilde{\mathbf{g}}_{mk}^T (\tilde{\mathbf{g}}_{mk}^T)^H\right\} \mathbf{t}_{mk}^{\text{ZF-Com}}\right\} \\ &= \sum_{m \in \mathcal{Z}_k} \sqrt{a_m \rho \eta_{mk}^c} \gamma_{mk} \sum_{m \in \mathcal{Z}_k} a_m \rho \eta_{mk}^c (\beta_{mk} - \gamma_{mk}) \\ &\quad \times \gamma_{mk}^2 \mathbb{E}\left\{[(\hat{\mathbf{G}}_{\mathcal{S}_m}^H \hat{\mathbf{G}}_{\mathcal{S}_m})^{-1}]_{kk}\right\} \\ &= \sum_{m \in \mathcal{Z}_k} \sqrt{a_m \rho \eta_{mk}^c} \gamma_{mk} \\ &\quad + \sum_{m \in \mathcal{Z}_k} a_m \rho \eta_{mk}^c (\beta_{mk} - \gamma_{mk}) \frac{\gamma_{mk}}{N - |\mathcal{S}_m|}. \end{aligned} \quad (75)$$

Then, the second term of (73), ϑ_M , can be derived as

$$\begin{aligned}\vartheta_M &= \sum_{m \in \mathcal{M}_k} a_m \rho \eta_{mk}^c \text{var} \left(\left(\|\hat{\mathbf{g}}_{mk}\|^2 + \tilde{\mathbf{g}}_{mk}^T \hat{\mathbf{g}}_{mk} \right) \right. \\ &\quad \left. + \left| \mathbb{E} \left\{ \sum_{m \in \mathcal{M}_k} a_m \sqrt{\rho \eta_{mk}^c} (\hat{\mathbf{g}}_{mk} + \tilde{\mathbf{g}}_{mk})^T \mathbf{t}_{mk}^{\text{MR-Com}} \right\} \right|^2 \right) \\ &= \sum_{m \in \mathcal{M}_k} a_m \rho \eta_{mk}^c N \gamma_{mk} \beta_{mk} \\ &\quad + \left(N \sum_{m \in \mathcal{M}_k} a_m \sqrt{\rho \eta_{mk}^c} \gamma_{mk} \right)^2.\end{aligned}\quad (76)$$

As a result, plugging (75) and (76) into (77), we have

$$\begin{aligned}\mathbb{E} \left\{ |\text{BU}_k|^2 \right\} &= \rho \sum_{m \in \mathcal{Z}_k} a_m \eta_{mk}^c (\beta_{mk} - \gamma_{mk}) \frac{\gamma_{mk}}{N - |\mathcal{S}_m|} \\ &\quad + \rho \sum_{m \in \mathcal{M}_k} N a_m \eta_{mk}^c \gamma_{mk} \beta_{mk}.\end{aligned}\quad (77)$$

The same steps can be followed to compute $\text{IUI}_{kk'}$:

$$\begin{aligned}\text{IUI}_{kk'} &= \rho \sum_{m \in \mathcal{Z}_k} a_m \eta_{mk'}^c (\beta_{mk'} - \gamma_{mk'}) \frac{\gamma_{mk'}}{N - |\mathcal{S}_m|} \\ &\quad + N \sum_{m \in \mathcal{M}_k} a_m \eta_{mk'}^c \gamma_{mk'} \beta_{mk'}.\end{aligned}\quad (78)$$

Moreover, by substituting (7) into (17d), taking expectation over $x_{r,ml}$, we get

$$\begin{aligned}\mathbb{E} \left\{ |\text{IR}_k|^2 \right\} &= \rho \sum_{m \in \mathcal{M}} \sum_{l \in \mathcal{L}} \rho \eta_{ml}^s (1 - a_m) \\ &\quad \times \mathbb{E} \left\{ \left| \mathbf{g}_{mk}^T \mathbf{a}_N(\phi_{t,ml}^a, \phi_{t,ml}^e) \right|^2 \right\}.\end{aligned}\quad (79)$$

Letting $\mathbf{A} = \mathbf{a}_N(\phi_{t,ml}^a, \phi_{t,ml}^e) \mathbf{a}_N^H(\phi_{t,ml}^a, \phi_{t,ml}^e)$, we have

$$\begin{aligned}\mathbb{E} \left\{ |\text{IR}_k|^2 \right\} &= \rho \sum_{m \in \mathcal{M}} \sum_{l \in \mathcal{L}} \eta_{ml}^s (1 - a_m) \mathbb{E} \left\{ \left| \mathbf{g}_{mk}^T \mathbf{A} \right|^2 \right\} \\ &= \rho \sum_{m \in \mathcal{M}} \sum_{l \in \mathcal{L}} \eta_{ml}^s (1 - a_m) \mathbb{E} \left\{ \mathbf{g}_{mk}^T \mathbf{A} \mathbf{g}_{mk}^* \right\} \\ &= \rho \sum_{m \in \mathcal{M}} \sum_{l \in \mathcal{L}} \eta_{ml}^s (1 - a_m) \beta_{mk} \text{tr}(\mathbf{A}),\end{aligned}\quad (80)$$

where $\text{tr}(\mathbf{A}) = N$. To this end, by substituting (71), (77), (78), and (80) into (19), the desired result in (21) is obtained. ■

REFERENCES

- [1] M. Elfiatoure, M. Mohammadi, H. Q. Ngo, and M. Matthaiou, "Cell-free massive MIMO for ISAC: Access point operation mode selection and power control," in *Proc. IEEE GLOBECOM*, Dec. 2023.
- [2] F. Liu, Y. Cui, C. Masouros, J. Xu, T. X. Han, Y. C. Eldar, and S. Buzzi, "Integrated sensing and communications: Toward dual-functional wireless networks for 6G and beyond," *IEEE J. Sel. Areas Commun.*, vol. 40, no. 6, pp. 1728–1767, Jun. 2022.
- [3] Z. Zhou, X. Li, J. He, X. Bi, Y. Chen, G. Wang, and P. Zhu, "6G integrated sensing and communication-sensing assisted environmental reconstruction and communication," in *Proc. IEEE ICASSP*, Jun. 2023, pp. 1–5.
- [4] M. Elfiatoure, M. Mohammadi, H. Q. Ngo, P. J. Smith, and M. Matthaiou, "Protecting massive MIMO-radar coexistence: Precoding design and power control," *IEEE Open J. Commun. Society*, vol. 5, pp. 276–293, Jan. 2024.
- [5] M. Elfiatoure, H. Q. Ngo, and M. Matthaiou, "Coexistence between massive MIMO and radar communications: Performance analysis," *J. Commun. Inf. Networks*, vol. 8, no. 1, pp. 37–47, Mar. 2023.
- [6] F. Liu, C. Masouros, A. Petropulu, H. Griffiths, and L. Hanzo, "Joint radar and communication design: Applications, state-of-the-art, and the road ahead," *IEEE Trans. Commun.*, vol. 68, no. 6, pp. 3834–3862, Jun. 2020.
- [7] F. Liu, L. Zhou, C. Masouros, A. Lit, W. Luo, and A. Petropulu, "Dual-functional cellular and radar transmission: Beyond coexistence," in *Proc. IEEE SPAWC*, Jun. 2018, pp. 1–5.
- [8] F. Liu, L. Zheng, Y. Cui, C. Masouros, A. P. Petropulu, H. Griffiths, and Y. C. Eldar, "Seventy years of radar and communications: The road from separation to integration," *IEEE IEEE Signal Process. Mag.*, vol. 40, no. 5, pp. 106–121, Jul. 2023.
- [9] F. Liu, C. Masouros, A. Li, H. Sun, and L. Hanzo, "MU-MIMO communications with MIMO radar: From co-existence to joint transmission," *IEEE Trans. Wireless Commun.*, vol. 17, no. 4, pp. 2755–2770, Apr. 2018.
- [10] A. Ali, N. Gonzalez-Prelcic, R. W. Heath, Jr., and A. Ghosh, "Leveraging sensing at the infrastructure for mmWave communication," *IEEE Commun. Mag.*, vol. 58, no. 7, pp. 84–89, Jul. 2020.
- [11] A. Zhang, M. L. Rahman, X. Huang, Y. J. Guo, S. Chen, and R. W. Heath, "Perceptive mobile networks: Cellular networks with radio vision via joint communication and radar sensing," *IEEE Veh. Technol. Mag.*, vol. 16, no. 2, pp. 20–30, Jun. 2020.
- [12] M. Temiz, E. Alsusa, and M. W. Baidas, "A dual-functional massive MIMO OFDM communication and radar transmitter architecture," *IEEE Trans. Technol.*, vol. 69, no. 12, pp. 14974–14988, Dec. 2020.
- [13] —, "Optimized precoders for massive MIMO OFDM dual radar-communication systems," *IEEE Trans. Commun.*, vol. 69, no. 7, pp. 4781–4794, Jul. 2021.
- [14] —, "A dual-function massive MIMO uplink OFDM communication and radar architecture," *IEEE Trans. Cognit. Commun. Netw.*, vol. 8, no. 2, pp. 750–762, Jun. 2021.
- [15] H. Q. Ngo, G. Interdonato, E. G. Larsson, G. Caire, and J. G. Andrews, "Ultra-dense cell-free massive MIMO for 6G: Technical overview and open questions," *Proc. IEEE, arXiv preprint arXiv:2401.03898*, 2024.
- [16] M. Matthaiou *et al.*, "The road to 6G: Ten physical layer challenges for communications engineers," *IEEE Commun. Mag.*, vol. 59, no. 1, pp. 64–69, Jan. 2021.
- [17] H. Q. Ngo, A. Ashikhmin, H. Yang, E. G. Larsson, and T. L. Marzetta, "Cell-free massive MIMO versus small cells," *IEEE Trans. Wireless Commun.*, vol. 16, no. 3, pp. 1834–1850, Mar. 2017.
- [18] J. Zhang, E. Björnson, M. Matthaiou, D. W. K. Ng, H. Yang, and D. J. Love, "Prospective multiple antenna technologies for beyond 5G," *IEEE J. Sel. Areas Commun.*, vol. 38, no. 8, pp. 1637–1660, Aug. 2020.
- [19] F. Zeng, J. Yu, J. Li, F. Liu, D. Wang, and X. You, "Integrated sensing and communication for network-assisted full-duplex cell-free distributed massive MIMO systems," *arXiv preprint arXiv:2311.05101*, 2023.
- [20] Z. Behdad, O. T. Demir, K. W. Sung, E. Björnson, and C. Cavdar, "Power allocation for joint communication and sensing in cell-free massive MIMO," in *Proc. IEEE GLOBECOM*, Dec. 2022, pp. 4081–4086.
- [21] U. Demirhan and A. Alkhateeb, "Cell-free ISAC MIMO systems: Joint sensing and communication beamforming," *arXiv preprint arXiv:2301.11328*, 2023.
- [22] W. Mao *et al.*, "Beamforming design in cell-free massive MIMO integrated sensing and communication systems," in *Proc. IEEE GLOBECOM*, Dec. 2023, pp. 546–551.
- [23] I. W. da Silva, D. P. Osorio, and M. Juntti, "Multi-static ISAC in cell-free massive MIMO: Precoder design and privacy assessment," in *Proc. IEEE GLOBECOM*, Dec. 2023, pp. 461–466.
- [24] G. Interdonato, M. Karlsson, E. Björnson, and E. G. Larsson, "Local partial zero-forcing precoding for cell-free massive MIMO," *IEEE Trans. Wireless Commun.*, vol. 19, no. 7, pp. 4758–4774, Apr. 2020.
- [25] H. Q. Ngo, L.-N. Tran, T. Q. Duong, M. Matthaiou, and E. G. Larsson, "On the total energy efficiency of cell-free massive MIMO," *IEEE Trans. Green Commun. and Networking*, vol. 2, no. 1, pp. 25–39, Mar. 2018.
- [26] B. Liao, H. Q. Ngo, M. Matthaiou, and P. J. Smith, "Low-complexity transmit beamforming design for massive MIMO-ISAC systems," in *Proc. IEEE GLOBECOM*, Dec. 2023, pp. 540–545.
- [27] H. Cramér, *Random Variables and Probability Distributions*. Cambridge University Press, 2004, no. 36.
- [28] H. Q. Ngo, E. G. Larsson, and T. L. Marzetta, "Energy and spectral efficiency of very large multiuser MIMO systems," *IEEE Trans. Commun.*, vol. 61, no. 4, pp. 1436–1449, Apr. 2013.
- [29] M. Grant and S. Boyd, "CVX: Matlab software for disciplined convex programming, version 2.1, [online]. available: <http://cvxr.com/cvx>, 2014.
- [30] T. T. Vu, D. T. Ngo, M. N. Dao, S. Durrani, and R. H. Middleton, "Spectral and energy efficiency maximization for content-centric C-RANs with edge caching," *IEEE Trans. Commun.*, vol. 66, no. 12, pp. 6628–6642, Dec. 2018.
- [31] H. H. M. Tam, H. D. Tuan, D. T. Ngo, T. Q. Duong, and H. V. Poor, "Joint load balancing and interference management for small-cell heterogeneous networks with limited backhaul capacity," *IEEE Trans. Wireless Commun.*, vol. 16, no. 2, pp. 872–884, Feb. 2017.
- [32] M. Mohammadi, T. T. Vu, H. Q. Ngo, and M. Matthaiou, "Network-assisted full-duplex cell-free massive MIMO: Spectral and energy efficiencies," *IEEE J. Sel. Areas Commun.*, vol. 41, no. 9, pp. 2833–2851, Sept. 2023.
- [33] E. Björnson and L. Sanguinetti, "Making cell-free massive MIMO competitive with MMSE processing and centralized implementation," *IEEE Trans. Wireless Commun.*, vol. 19, no. 1, pp. 77–90, Jan. 2020.